SAPIENZA
UNIVERSITÀ DI ROMA

DOTTORATO DI RICERCA IN ENERGIA E AMBIENTE
PhD Program in ENERGY and ENVIRONMENT

XXXVII Cycle

CFD study of the sanitization of surfaces by means of hydrogen peroxide vapour

PhD Thesis

Scuola di Dottorato in Scienze e Tecnologie per l'Innovazione Industriale
Facoltà di Ingegneria Civile e Industriale
Dipartimento di Ingegneria Astronautica, Elettrica ed Energetica

Gianluca Sbardella

Advisor
Prof. Annunziata D'Orazio

Co-Advisor/Tutor
Prof. Annunziata D'Orazio

A.A. 2025-2026

Table of Contents

Structure of the Thesis

This thesis is organised as follows.

Chapter 1, presents the general introduction, including public health context, engineering background and research objectives.

Chapter 2, describes the theoretical framework and numerical methodology, including governing equations, turbulence modelling and boundary conditions.

Chapter 3, presents the computational model and simulation setup for confined room geometries.

Chapter 4, discusses results related to vapour dispersion, study of the trend of hydrogen peroxide vapor concentration and aeration performance.

Chapter 5, provides conclusions, limitations and perspectives for future research.

Nomenclature

The following symbols and abbreviations are used throughout this thesis:

u, v, w — velocity components (m/s)

p — pressure (Pa)

ρ — fluid density (kg/m³)

μ — dynamic viscosity (Pa·s)

c — concentration of hydrogen peroxide (mol/m³)

D — molecular diffusion coefficient (m²/s)

Q — volumetric flow rate (m³/s)

V — volume of the domain (m³)

Re — Reynolds number

Pe — Péclet number

k — turbulent kinetic energy

ε — dissipation rate of turbulent kinetic energy

ω — specific dissipation rate

CFD — Computational Fluid Dynamics

VHP — Vaporised Hydrogen Peroxide

RANS — Reynolds-Averaged Navier–Stokes

SST — Shear Stress Transport

ACH — Air Changes per Hour

Chapter 1

Introduction

1.1 Global Health Context and Indoor Environmental Risk

In recent decades, the relationship between humans and the built environment has undergone a significant transformation. Increasing urbanisation, the shift of most working activities to indoor settings, and the growing complexity of healthcare systems have led to a situation in which the majority of daily activities occur within enclosed environments.

It is widely reported that individuals in industrialised countries spend approximately 80–90% of their time indoors (Klepeis et al., 2001). This observation highlights the central role of indoor environmental conditions in public health. Factors such as air quality, ventilation performance, surface contamination, and cleaning practices directly influence human exposure to biological and chemical hazards.

Healthcare-associated infections (HAIs) remain a major global concern. According to the World Health Organization (WHO, 2011), hundreds of millions of patients are affected each year worldwide. In European acute care hospitals, the prevalence of HAIs is estimated to be approximately 6% (ECDC, 2019). Although this percentage may appear moderate, the absolute number of cases is substantial, with significant consequences in terms of morbidity, mortality, and economic burden.

The COVID-19 pandemic further emphasised the importance of indoor environments in the transmission of infectious diseases. Several studies have shown that enclosed spaces such as offices, commercial areas, and public transport systems can facilitate

the spread of respiratory pathogens (Morawska and Cao, 2020). In these contexts, ventilation conditions, occupancy density, and surface contamination contribute to transmission dynamics.

For these reasons, environmental sanitisation should not be considered merely as a routine cleaning activity, but rather as an engineered intervention aimed at reducing exposure pathways and mitigating infection risk within confined environments.

1.2 Surface Contamination and Indirect Transmission Pathways

Microorganisms are capable of surviving on inanimate surfaces for extended periods, often longer than commonly assumed. (Kramer et al. 2006) reported that several nosocomial pathogens can persist on dry surfaces for days or even months, enabling indirect transmission through contact with contaminated surfaces.

High-touch surfaces such as bed rails, door handles, keyboards, and medical equipment represent critical points of contamination (Otter et al., 2013). Similar risk factors are present in non-hospital environments, including offices and commercial spaces, where shared surfaces and equipment are frequently used.

An additional complexity is introduced by the formation of biofilms, which are structured microbial communities embedded in a protective extracellular matrix (Hall-Stoodley et al., 2004). Biofilms significantly increase resistance to disinfectants and environmental stress, reducing the effectiveness of conventional cleaning methods.

Manual sanitisation procedures are inherently dependent on human performance and may lead to incomplete coverage (Carling et al., 2008). Studies have shown that even in controlled hospital environments, cleaning practices often leave untreated areas (Carling et al., 2008). In less controlled settings, variability is likely to be even greater.

From an engineering perspective, surface sanitisation should be interpreted as a transport problem rather than solely a chemical process. The disinfectant must be delivered to the surface, maintained in contact for a sufficient duration, and subsequently removed in a controlled manner. This perspective motivates the adoption of automated and whole-room sanitisation technologies.

1.3 Environmental Hygiene and Antimicrobial Resistance

Antimicrobial resistance (AMR) is widely recognised as one of the most significant threats to global health (WHO, 2023). Resistant microorganisms are more difficult to treat and can persist in the environment for prolonged periods, contributing to ongoing transmission.

Environmental contamination plays an indirect but important role in the spread of AMR. When resistant organisms remain on surfaces, transmission between individuals may occur without direct contact. Each resulting infection may require antibiotic treatment, increasing selective pressure and further promoting resistance development.

Environmental hygiene therefore represents a complementary strategy in the mitigation of AMR. By reducing microbial load in indoor environments, it is possible to decrease infection rates and consequently limit antibiotic usage. Although environmental interventions alone cannot solve the problem, they form part of a multi-layered approach to infection control.

In this context, high-level disinfectants capable of inactivating resistant microorganisms are of particular importance. Among these, hydrogen peroxide has gained attention due to its broad-spectrum antimicrobial activity and favourable environmental profile.

1.4 Hydrogen Peroxide as a High-Level Decontamination Agent

Hydrogen peroxide (H_2O_2) is widely used as an antiseptic and disinfectant due to its strong oxidising properties. Its antimicrobial activity is based on the generation of reactive oxygen species, which can damage cellular membranes, denature proteins, and disrupt nucleic acids (Linley et al., 2012).

One of the key advantages of hydrogen peroxide lies in its decomposition into water and oxygen:

$$2H_2O_2 \rightarrow 2H_2O + O_2$$

This reaction ensures that no persistent toxic residues remain after use, making hydrogen peroxide environmentally preferable compared to other disinfectants such as chlorine-based compounds or aldehydes.

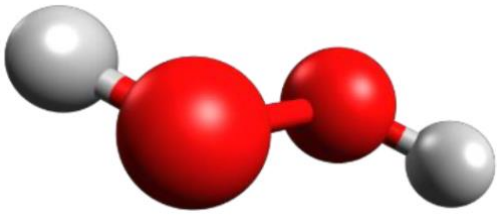

Figure 1 Hydrogen peroxide

Hydrogen peroxide exhibits broad-spectrum antimicrobial activity, being effective against bacteria, viruses, fungi, and bacterial spores (McDonnell and Russell, 1999). In healthcare settings, it has demonstrated efficacy against clinically relevant pathogens such as Clostridioides difficile and methicillin-resistant Staphylococcus aureus (MRSA) (Otter et al., 2007).

Despite these advantages, hydrogen peroxide is not without limitations. At elevated concentrations, it may cause irritation to the eyes, skin, and respiratory tract. For this reason, occupational exposure limits have been established. The Occupational Safety and Health Administration (OSHA, 2023) defines a permissible exposure limit of 1 ppm as an 8-hour time-weighted average.

These considerations highlight the importance of controlling both concentration and exposure time during sanitisation processes, particularly in enclosed environments.

1.5 Vaporised Hydrogen Peroxide for Surface Sanitisation

The development of vaporised hydrogen peroxide (VHP) systems represents a significant advancement in environmental sanitisation technologies. When hydrogen peroxide is vaporised under controlled temperature and humidity conditions, it behaves similarly to a gas, allowing for more uniform distribution within enclosed spaces.

Table 1
Comparison of the Sterinis aerosolised hydrogen peroxide, Steris vaporised hydrogen peroxide and Bioquell hydrogen peroxide vapour systems

	Sterinis	Steris	Bioquell
Name	Aerosolised[7]/'dry mist'[1,6] hydrogen peroxide	Vaporised hydrogen peroxide[2]	Hydrogen peroxide vapour[8]
Abbreviation	DMHP[1]	VHP®[2]	HPV[8]
Active solution	Sterusil® (5% hydrogen peroxide, <50 ppm silver cations, <50 ppm *ortho*-phosphoric acid)	Vaprox® (35% hydrogen peroxide)	35% hydrogen peroxide
Application	Aerosol of active solution	Vapour, non-condensing	Vapour, condensing
Particle size	8–10 μm[6]	Vapour phase	Vapour phase
Aeration (removal of active from enclosure)	Passive decomposition	Active catalytic conversion	Active catalytic conversion
Sporicidal efficacy	Single cycle does not inactivate *Bacillus atrophaeus* BIs;[7] ~4 $\log_{10}$ reduction of *C. difficile in vitro* and incomplete inactivation *in situ*[5,6]	*Geobacillus stearothermophilus* BIs routinely used to verify cycle efficacy[2]	*Geobacillus stearothermophilus* BIs routinely used to verify cycle efficacy;[4,9] > 6 $\log_{10}$ reduction of *C. difficile in vitro* and complete inactivation *in situ*[8,9]
Tuberculocidal efficacy	Unclear[1,3]	Yes[2]	Yes[4]
UK Rapid Review Panel Recommendation	3: 'A potentially useful new concept but insufficiently validated; more research and development is required before it is ready for evaluation in practice.'	2: 'Basic research and development has been completed and the product may have potential value; in use evaluations/trials are now needed in an NHS clinical setting.'	1: 'Basic research and development, validation and recent in use evaluations have shown benefits that should be available to NHS bodies to include as appropriate in their cleaning, hygiene or infection control protocols.'
Evidence of clinical impact	None published	None published	Significant reduction in the incidence of *C. difficile* and VRE.[5,9,10]

BI, biological indicator; NHS, National Health Service; VRE, vancomycin-resistant enterococci.

Table 1. Comparison between DMHP, HPV and VHP sanitisation technologies.

A typical VHP sanitisation cycle consists of four main phases: conditioning, injection, dwell, and aeration (Hall et al., 2007; Otter et al., 2007). During the injection phase, the vapour concentration increases until a target level is reached. The dwell phase allows sufficient contact time for microbial inactivation, while the aeration phase ensures removal of the vapour to safe levels prior to re-entry. Compared to manual cleaning procedures, VHP systems offer several advantages, including reduced operator dependency, improved penetration into complex geometries, and enhanced reproducibility of sanitisation cycles (Boyce et al., 2008).

These features make VHP particularly suitable for environments where uniform coverage is difficult to achieve through manual methods.
However, uniform sanitisation cannot be assumed a priori (Chen, 2009). The effectiveness of VHP depends on its ability to reach all surfaces and maintain adequate exposure conditions. This process is governed by airflow patterns within the environment, which determine the transport and distribution of the vapour.

	Micro-organism	Effect in log_{10} reduction, median (range)	N (ref)
Viruses	Norovirus	2.5 (0.5–2.7)	3 [12, 18, 19]
	(Surrogate)	4.5 (> 4–5.3)	3 [18–20]
Bacteria	*Acinetobacter*	2 (1–>4)	2 [12, 16]
	CPE		
	VRE	1–1.7	1 [21]
	ESBL	> 6	1 [14]
	MRSA	> 4 (2–>6)	4 [12, 14, 16, 17]
Spores	*C. difficile*	4.9 (0.13–>5)	4 [12, 14, 22, 23]
Yeast	*C. auris*		

Table 2. In vitro efficacy of aHP against some microorganisms, expressed in log-reduction

In confined spaces, airflow is influenced by ventilation systems, obstacles, and thermal effects, leading to the formation of recirculation zones and regions of reduced mixing. These phenomena may significantly affect both the distribution and deposition of hydrogen peroxide vapour.
For this reason, understanding the behaviour of VHP in indoor environments requires an engineering approach capable of describing the interaction between airflow and species transport.

1.6 Multiphysics Behaviour of VHP in Confined Environments

The sanitisation of surfaces using hydrogen peroxide vapour is inherently a multiphysics process involving several coupled phenomena. These include fluid dynamics, turbulent transport, molecular diffusion, and interaction between vapour and solid surfaces.

In mechanically ventilated indoor environments, airflow is typically turbulent, characterised by complex velocity fields, recirculation zones, and time-dependent fluctuations (Awbi, 2003; Chen, 2009). Under these conditions, convective transport generally dominates over molecular diffusion, leading to strong dependence of vapour distribution on airflow structure.

Surface sanitisation is influenced not only by airborne concentration but also by local exposure conditions, including contact time and accessibility (Nielsen, 2015). Surfaces that are shielded from the main airflow or located within stagnant regions may receive insufficient exposure, potentially compromising sanitisation effectiveness.

In addition, condensation phenomena may occur under certain conditions, altering local concentration and interaction mechanisms (Chen, 2009). Although not always dominant, these effects may contribute to non-uniform behaviour in real environments.

The removal phase introduces further complexity. After the dwell period, hydrogen peroxide vapour must be efficiently removed through ventilation or catalytic decomposition systems. However, clearance is not necessarily uniform across the domain, and localised regions of higher concentration may persist.

The combination of these processes highlights the need for modelling tools capable of capturing their coupled behaviour. Computational Fluid Dynamics (CFD) provides a suitable framework for analysing airflow and species transport simultaneously within confined environments.

1.7 Human Exposure and Toxicological Considerations

While hydrogen peroxide offers several advantages as a sanitising agent, its potential impact on human health must be carefully considered. The same oxidative properties responsible for microbial inactivation may cause irritation if exposure levels exceed safety thresholds.

Hydrogen peroxide vapour can affect the eyes, skin, and respiratory system (ATSDR, 2002). Acute exposure to high concentrations may lead to symptoms such as coughing, throat irritation, and mucosal discomfort (ATSDR, 2002). For occupational settings, exposure limits have been established to minimise health risks. The (OSHA, 2023) permissible exposure limit of 1 ppm represents a widely adopted reference value.

During VHP sanitisation cycles, concentrations may exceed these limits by several orders of magnitude, particularly during injection and dwell phases. For this reason, treated environments must remain unoccupied during operation. However, the critical phase from a safety perspective is often the aeration phase.

If removal of hydrogen peroxide vapour is not spatially uniform, localised regions with elevated concentration may persist even when average values indicate safe conditions (Nielsen, 2015). In confined environments with complex geometry, such as hospital rooms or open-plan offices, stagnation zones may significantly delay clearance.

These considerations highlight that toxicological safety cannot be assessed solely on the basis of average concentration measurements. Instead, spatial variability must be taken into account.

In this context, CFD modelling plays a crucial role not only in analysing sanitisation effectiveness but also in supporting safety assessment and optimisation of re-entry conditions.

1.8 Removal and Aeration Mechanisms of Hydrogen Peroxide

The sanitisation process based on vaporised hydrogen peroxide can be conceptually divided into two main phases: distribution and removal. While the distribution phase is directly associated with microbial inactivation, the removal phase is equally critical from a safety perspective.

Following the dwell period, hydrogen peroxide concentration must be reduced below regulatory thresholds before the environment can be safely reoccupied. This process is typically achieved through a combination of mechanisms, including forced ventilation with increased air exchange rates, catalytic decomposition systems that convert hydrogen peroxide into water and oxygen, adsorption processes, and real-time monitoring using chemical sensors.

The efficiency of the removal phase depends on several interacting parameters, such as room geometry, ventilation rate, airflow patterns, and initial vapour concentration (Chen, 2009). These factors are not independent; for example, increasing ventilation rate may alter airflow structures, thereby affecting local concentration gradients.

In confined environments, removal cannot be considered a purely temporal decay process. Instead, it is governed by spatially dependent transport phenomena. Regions characterised by weak airflow or recirculation may exhibit slower concentration decay, leading to delayed clearance (Nielsen, 2015).

For this reason, the estimation of safe re-entry conditions based solely on average concentration measurements may be insufficient (Chen, 2009). A spatially resolved analysis is required to identify potential critical zones and ensure that safety thresholds are satisfied throughout the entire domain.

Computational Fluid Dynamics (CFD) provides a suitable framework for analysing these processes, enabling the investigation of both temporal and spatial aspects of vapour removal.

1.9 Application in Non-Hospital Environments: Offices, Commercial and Public Spaces

Although vaporised hydrogen peroxide technology has been primarily developed for healthcare and pharmaceutical applications, its potential use in non-hospital environments has gained increasing attention.

Indoor spaces such as offices, commercial buildings, transportation hubs, and educational facilities are characterised by high occupancy levels, shared surfaces, and prolonged exposure times (Klepeis et al., 2001). These environments present conditions that may facilitate the transmission of infectious agents, particularly in the presence of inadequate ventilation.

The COVID-19 pandemic has highlighted the vulnerability of such environments, demonstrating how clusters of infection may originate in offices, commercial spaces, and other indoor settings (Hamner et al., 2020). In many cases, ventilation systems are designed primarily for thermal comfort rather than for infection control (Awbi, 2003).

In this context, periodic whole-room sanitisation using VHP may represent an additional preventive strategy, particularly following confirmed contamination events. Compared to manual cleaning, automated vapour-based systems offer improved coverage and reduced dependency on operator performance.

However, the application of VHP in non-hospital environments introduces additional constraints. Operational downtime must be minimised, and re-entry conditions must be predictable and safe. These requirements emphasise the importance of accurately modelling both vapour distribution and removal phases.

Furthermore, occupants in non-healthcare environments may not expect exposure to chemical agents, making safety considerations even more critical. As a result, the design and optimisation of sanitisation protocols must balance effectiveness with minimal disruption and maximum safety.

1.10 CFD Modelling of Vapour Dispersion in Confined Rooms

The analysis of hydrogen peroxide vapour behaviour in confined environments requires modelling tools capable of describing airflow and species transport simultaneously. Computational Fluid Dynamics (CFD) provides such capability, enabling detailed investigation of multiphysics processes within indoor spaces.

CFD is based on the numerical solution of the governing equations of fluid motion and scalar transport (Versteeg and Malalasekera, 2007). In indoor applications, airflow is typically described by the incompressible Navier–Stokes equations, coupled with a transport equation for vapour concentration.

In mechanically ventilated environments, flow conditions are generally turbulent, requiring the adoption of appropriate turbulence modelling approaches. Reynolds-Averaged Navier–Stokes (RANS) models are commonly used in indoor airflow simulations due to their balance between computational efficiency and predictive capability.

From a modelling perspective, the sanitisation process involves two coupled phenomena: transport of vapour within the air volume and interaction between vapour and solid surfaces (Chen, 2009).

The spatial distribution of vapour is strongly influenced by room geometry, including walls, ventilation systems, and internal obstacles such as furniture (Nielsen, 2015). These elements generate complex airflow patterns, including jets, recirculation zones, and stagnation regions.

CFD simulations allow the analysis of temporal evolution of vapour concentration, spatial distribution of exposure, identification of poorly ventilated regions, and concentration decay during the aeration phase.

Such analyses provide valuable insights for the optimisation of sanitisation protocols and contribute to a more accurate understanding of the physical processes governing VHP behaviour in real environments.

1.11 Regulatory Framework and Safety Guidelines

The implementation of hydrogen peroxide-based sanitisation systems is subject to regulatory frameworks and safety guidelines established by international and national organisations.

The World Health Organization (WHO, 2011) recognises environmental hygiene as a key component of infection prevention strategies. Similarly, the European Centre for Disease Prevention and Control (ECDC, 2019) provides guidance on infection control practices, including environmental cleaning and disinfection.

In the United States, the Centers for Disease Control and Prevention (CDC, 2022) issues recommendations on disinfection and sterilisation procedures in healthcare settings. These guidelines define acceptable practices but generally do not address detailed airflow-dependent phenomena.

From an occupational safety perspective, exposure limits for hydrogen peroxide are defined by regulatory agencies such as OSHA (2023) and the European Chemicals Agency (ECHA, 2021). These limits are intended to protect workers and occupants from adverse health effects.

However, regulatory frameworks typically provide threshold values without accounting for spatial variability in concentration within complex indoor environments (Chen, 2009). As a result, compliance with average concentration limits does not necessarily guarantee uniform safety conditions throughout a space.

In this context, engineering tools such as CFD can support the translation of regulatory requirements into practical design criteria, enabling the assessment of spatial concentration fields and identification of potential critical zones.

1.12 Scientific Gaps in Literature

The previous sections have outlined the complexity of hydrogen peroxide vapour (VHP) sanitisation processes, highlighting the interplay between microbiological efficacy, fluid-dynamic transport, and safety constraints in confined indoor

environments. Within this context, a critical analysis of the existing literature reveals several limitations that justify the need for further investigation.

The majority of studies on VHP focus on microbiological efficacy, demonstrating the capability of hydrogen peroxide to inactivate a broad spectrum of pathogens under controlled conditions (McDonnell and Russell, 1999; Boyce et al., 2008). These contributions are essential for validating the effectiveness of the disinfectant itself; however, they typically rely on experimental indicators and provide limited insight into the physical mechanisms governing vapour distribution.

From an engineering perspective, the behaviour of hydrogen peroxide vapour is fundamentally determined by airflow patterns, turbulence structures, and room geometry. Extensive research in indoor air quality has shown that contaminant transport in confined environments is strongly influenced by ventilation design and flow topology (Chen, 2009; Nielsen, 2015). Nevertheless, only a limited number of studies have explicitly addressed VHP within a CFD framework, and even fewer have considered realistic indoor configurations with geometric complexity.

A significant limitation of the current literature lies in the simplified representation of sanitisation processes. In many cases, vapour distribution is assumed to be spatially uniform, or the analysis is restricted to steady-state conditions. Such assumptions neglect the transient nature of real VHP cycles, which involve distinct injection, dwell, and aeration phases (Chen, 2009). As a result, important phenomena such as delayed mixing, local concentration gradients, and time-dependent exposure conditions are often overlooked.

Another critical gap concerns the weak coupling between airborne concentration fields and surface exposure (Nielsen, 2015). In several studies, sanitisation effectiveness is implicitly correlated with average concentration levels, without explicitly accounting for spatial variability or shielding effects caused by obstacles. However, as discussed in previous sections, surfaces located in recirculation zones or poorly ventilated regions may experience significantly different exposure conditions compared to well-mixed areas (Nielsen, 2015).

Furthermore, the aeration phase remains underrepresented in the literature (Noakes et al., 2006). While considerable attention is typically devoted to achieving target concentration levels during the distribution phase, the removal of hydrogen peroxide vapour is often treated as a secondary process. This represents a significant limitation, as spatial variability during clearance directly affects safe re-entry conditions. Localised regions of elevated concentration may persist even when average values comply with regulatory thresholds.

These observations highlight the need for a more comprehensive modelling approach capable of integrating the multiple physical processes involved in VHP sanitisation. In particular, the following gaps can be identified: limited CFD-based studies specifically focused on VHP behaviour in confined environments; insufficient analysis of transient sanitisation cycles, including injection, dwell, and aeration phases; lack of detailed coupling between airflow dynamics, vapour transport, and surface exposure conditions; limited consideration of spatial heterogeneity and shielding effects due to internal geometry; insufficient investigation of vapour removal and its implications for safe re-entry (Chen, 2009).

The present research aims to address these gaps by developing a CFD-based framework for the analysis of hydrogen peroxide vapour in confined indoor environments. By integrating turbulent airflow modelling with species transport and spatially resolved concentration analysis, this study provides a more realistic representation of both distribution and removal processes.

In this way, the work contributes to bridging the gap between experimental validation of sanitisation efficacy and engineering-based prediction of vapour behaviour, supporting the design of more effective and safer VHP sanitisation protocols.

1.13 Research Objectives and Contribution of This PhD

The primary objective of this doctoral research is to develop a CFD-based framework for analysing the sanitisation of surfaces using hydrogen peroxide vapour in confined environments. In particular, the study seeks to simulate vapour dispersion within

representative indoor geometries, evaluate the exposure conditions of surfaces, and analyse the spatial variability of concentration. It also aims to investigate removal dynamics and aeration efficiency, as well as assess the implications for safe re-entry following sanitisation procedures.

The main contribution of this work lies in the integration of air-phase transport modelling with surface interaction considerations within a unified computational approach. By focusing on confined environments, the research addresses realistic scenarios commonly encountered in healthcare, laboratory, and commercial settings.

Chapter 2

2.1 Computational Fluid Dynamics

The sanitisation of confined indoor environments by means of hydrogen peroxide vapour is governed primarily by fluid-dynamic transport phenomena. The spatial distribution of vapour concentration, its interaction with surfaces, and its removal during aeration are strongly influenced by airflow patterns, turbulence intensity, and ventilation efficiency. For this reason, Computational Fluid Dynamics (CFD) is adopted in this work as the main methodological framework.

Over the past decades, CFD has become a widely established tool in engineering applications, including indoor environmental analysis, airborne contaminant transport, and infection control studies (Chen, 2009; Nielsen, 2015). Its main advantage lies in the capability to resolve three-dimensional, time-dependent fields of

velocity, pressure, and scalar concentration, providing detailed spatial information that cannot be obtained through experimental measurements alone.
Experimental investigations remain essential for validation purposes; however, they are inherently limited to discrete measurement points. In contrast, CFD enables full-field analysis and allows systematic parametric studies under controlled conditions. The integration of experimental and numerical approaches is therefore considered a robust strategy in indoor environmental engineering.
From a theoretical standpoint, CFD is based on the conservation equations of continuum mechanics. Under typical indoor conditions, airflow can be reasonably assumed incompressible due to low Mach numbers and negligible density variations (Awbi, 2003).
The conservation of mass is expressed by the continuity equation:

$$\nabla \cdot u = 0 \tag{1}$$

where u denotes the velocity vector field.
The conservation of momentum is described by the incompressible Navier–Stokes equations:

$$\rho \left(\frac{\partial u}{\partial t} + u \cdot \nabla u \right) = -\nabla p + \mu \nabla^2 u + f \tag{2}$$

where ρ is the fluid density, p is the static pressure, μ is the dynamic viscosity, and u is the velocity vector field.
The non-linear convective term introduces strong coupling between velocity components and is responsible for the development of complex flow structures (Versteeg and Malalasekera, 2007). In mechanically ventilated indoor environments, the Reynolds number typically indicates turbulent flow conditions (Awbi, 2003).

Under such conditions, inertial forces dominate viscous effects, leading to chaotic and multi-scale flow behaviour.

The computational domain considered in this study represents a confined indoor space equipped with mechanical ventilation (Awbi, 2003). The geometry includes supply and exhaust vents, as well as internal obstacles such as furniture. These elements significantly influence airflow structure, generating recirculation zones, shear layers, and stagnation regions that directly affect vapour transport (Chen, 2009).

Direct Numerical Simulation (DNS), which resolves all turbulent scales, is computationally unfeasible for room-scale applications due to the high Reynolds numbers involved. Therefore, turbulence modelling approaches are required, as discussed in the following section.

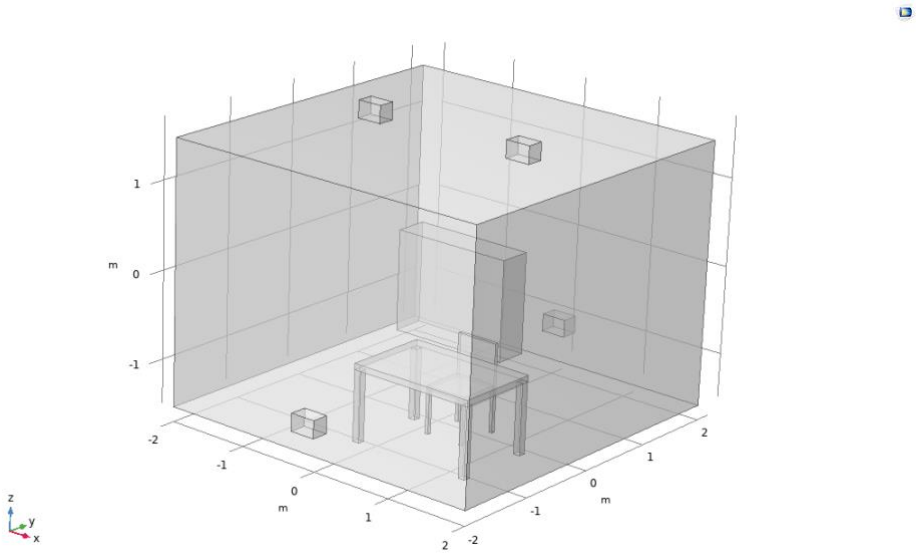

Figure 2. Geometry

Resolving all turbulent scales through Direct Numerical Simulation (DNS) would require extremely fine spatial and temporal resolution, rendering it computationally prohibitive for room-scale domains. Consequently, practical modelling relies on turbulence modelling strategies.

2.2 Turbulence Modelling

The equations that govern a generic 3D compressible flow are the Navier–Stokes equations which, as already mentioned, constitute a closed system independently from the laminar or turbulent nature of the flow. The above equations, however, are not linear because of the corrective term and therefore produce nonlinear multiscale dynamics: one important effect is exactly turbulence.

In fluid dynamics, the turbulent flow regime is characterized by an unstable motion highly irregular of a large number of vortices that vary considerably in their dimensions and interact with each other in a random way (Hinze, 1975). While laminar flows are stable, turbulent flows are chaotic, time-dependent and involve fluctuations of vorticity and three-dimensional velocity over wide scales of length and time. Turbulence is not a physical property of the fluid, but a phenomenon caused by the multiscale nature of the fluid motion at high Reynolds numbers: all flows become unstable above a certain Reynolds number, which represents the ratio between inertial forces and viscous forces (Pope, 2000).

$$Re = \frac{\rho u L}{\mu} \tag{3}$$

With the increase of Reynolds number the inertia increases with respect to viscous forces, therefore beyond a certain critical Re an unstable motion is established where the velocity profile stops to be parabolic, leading to a turbulent mode, a chaotic regime characterized by numerous vortices interconnected with each other.

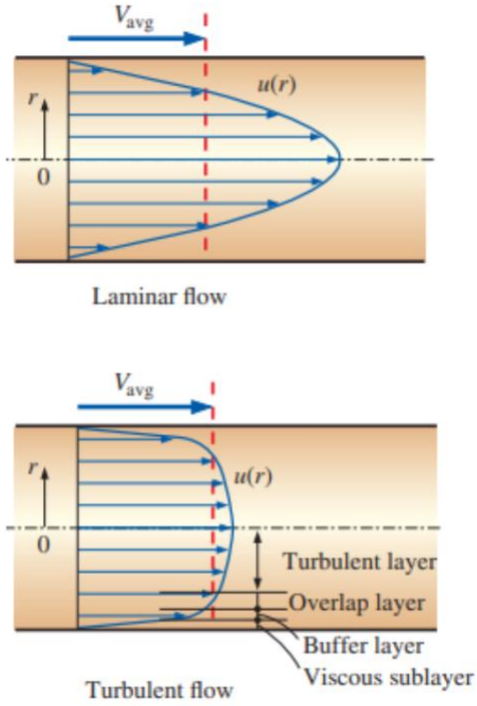

Figure 3. Representation of laminar and turbulent flow

Julius Oscar Hinze, a scientist known for his studies on fluid dynamics, defined the turbulent motion of a fluid as follows: "it is an irregular condition of flow in which the various quantities show a random variation with the coordinates of time and space, in such a way that statistically distinct mean values can be discerned".
As already mentioned, in principle, the transient 3D Navier–Stokes equations are valid both for laminar and turbulent flows. With the Direct Numerical Simulation (DNS) the turbulence is simulated without introducing any model, solving directly the Navier–Stokes equations: this is why this is the most accurate possible simulation method. However, the direct numerical simulation (DNS) of turbulence requires that the mesh size is sufficiently fine to resolve the smallest scales of the turbulent flow motion. Even today, the DNS approach is feasible only for moderately high Reynolds numbers, since the mesh size h scales with the Reynolds number as $Re^{\frac{9}{4}}$ and the time step Δt depends on it as $Re^{-\frac{1}{2}}$. Consequently, the DNS cost tends to become prohibitive with the increase of Reynolds number. The total computational cost for

turbulent flows without walls is then equal to $C \propto Re^3$. For wall bounded turbulent flows the cost is even higher, $C \propto Re^{3.4}$.

If the presence of microscopic turbulent vortices makes DNS too expensive, the fine scale effects not resolvable can be eliminated by filtering (averaging) the Navier–Stokes equations.

The most popular turbulence models of this type are based on the Reynolds Averaged Navier–Stokes (RANS) equations (Pope, 2000; Wilcox, 2006). The modeling based on RANS renounces to the exact treatment of turbulence in order to determine a mean field in space and time. RANS models are based on the Reynolds decomposition, which separates a flow variable (such as velocity u) into two components: a time-mean component ($\bar{u}$) and a fluctuating component u'. Once the Navier–Stokes equations are time averaged, the RANS equations are obtained which however contain new terms called Reynolds stresses, that represent the effect of turbulent fluctuations.

Let us now see how the RANS are obtained starting from the Navier–Stokes equations.

The statistical mean of a generic variable φ is indicated with $\bar{\varphi}$. The instantaneous deviation from the mean is written as $\varphi' = \varphi - \bar{\varphi}$. By definition, the time mean $\bar{\varphi}'$of a fluctuation φ' is equal to zero. Moreover, the time mean of a partial derivative is equal to the partial derivative of the time mean of the same variable, that is:

$$\overline{\frac{\partial \varphi}{\partial t}} = \frac{\partial \bar{\varphi}}{\partial t}, \quad \frac{\partial \bar{\varphi}}{\partial \overline{x_k}} = \frac{\partial \bar{\varphi}}{\partial x_k}, \quad k = 1,2,3 \tag{4}$$

In this specific case the variable φ would be specified for example in the pressure field or one component of velocity. Therefore, reporting the general form of the Navier–Stokes equation for incompressible fluids, one has:

$$\rho \frac{\partial u}{\partial t} + \rho\, u \cdot \nabla u - \nabla \cdot (2\,\mu\,\varepsilon) + \nabla p_g = 0 \tag{5}$$

$$\nabla \cdot u = 0, \quad \varepsilon = \frac{1}{2}(\nabla u + \nabla u^T) \tag{6}$$

For simplicity it is assumed that density ρ is constant and also viscosity μ. This expression is slightly different from the one reported in the previous paragraph because the external forces, in this case the gravity force ρg, have been incorporated into the modified pressure p_g. For what stated before regarding the generic variable φ, one can write the instantaneous velocity as $u = \bar{u} + u'$ and moreover the mean of the divergence of u will be equal also to $\nabla \cdot \bar{u} = 0$. By definition therefore the mean velocity field ū is divergence-free, that is:

$$\nabla \cdot \bar{u} = 0 \tag{7}$$

In other words, for incompressible flow, the mean field is solenoidal, that is it has zero divergence, and this implies consequently that also the divergence of the fluctuation field will be zero. What just described regarding the derivative of the mean and the mean of the derivative, it applies also to gradients and for this reason the terms of the equation become:

$$\frac{\partial \bar{u}}{\partial t} = \frac{\partial \bar{u}}{\partial t}, \quad \nabla \bar{u} = \nabla \bar{u}, \quad \nabla \overline{p_g} = \nabla \bar{p}_g, \quad \nabla \overline{(2\,\mu\,\varepsilon)} = \nabla \cdot [\mu(\nabla \bar{u} + \nabla \bar{u}^T)] \tag{8}$$

The only term that differs once averaged is $\rho\, u \cdot \nabla u$. Substituting $u = \bar{u} + u'$ in the equivalent conservative form $\nabla \cdot (\rho\, u \otimes u)$, one obtains:

$$\rho\, \bar{u} \cdot \nabla \bar{u} = \rho\, \bar{u} \cdot \nabla \bar{u} - \nabla \cdot \bar{\bar{\tau}} \tag{9}$$

where $\bar{\bar{\tau}}$ is the Reynolds Stress Tensor, which represents the transport of momentum due to turbulent fluctuations and is defined as:

$$\bar{\bar{\tau}} = -\overline{\rho\, u' \otimes (u')} \tag{10}$$

One finally arrives to the RANS:

$$\rho \frac{\partial \bar{u}}{\partial t} + \rho\, \bar{u} \cdot \nabla \bar{u} - \nabla \cdot [\mu(\nabla \bar{u} + \nabla \bar{u}^T) + \bar{\bar{\tau}}] + \nabla \bar{p}_g = 0 \tag{11}$$

Therefore one obtains equations that are formally similar to the starting Navier–Stokes equations, except for the fact that all quantities are mean values and for the presence of the additional term that derives from the nonlinearity of the convective term, whose diagonal components represent the normal stresses and the off-diagonal ones instead the shear stresses. The motion equations so averaged still provide an exact description of the mean scales of the turbulent flow, but constitutive equations must be provided for the turbulent stresses:

$$\tau_{ij} = -\rho\, u_i' \overline{u_j'} = \begin{pmatrix} \overline{u'^2} & \overline{u'v'} & \overline{u'w'} \\ \overline{u'v'} & \overline{v'^2} & \overline{v'w'} \\ \overline{u'w'} & \overline{v'w'} & \overline{w'^2} \end{pmatrix} \tag{12}$$

The Reynolds stress tensor $\bar{\bar{\tau}} = \{\tau_{ij}\}$ is symmetric. Moreover, it does not depend on the fluid or on its properties in general, but on the flow, that is on the specific type of problem, therefore one does not have a universal description of this term.
The closure problem of the RANS equations is a central challenge in computational fluid dynamics when trying to simulate turbulent flows, because the number of unknowns is greater than the number of equations available (closure problem); this implies that the system is not solvable in closed way. The closure problem in the RANS equations leads to the necessity of modelling the Reynolds stresses in such a way that the equations become "closed", that is that the number of available equations corresponds to the number of unknowns. Without a closure model, it is not possible to solve the equations to obtain the behaviour of the turbulent flow.
In practice, the closure problem reduces to determine a model that expresses the Reynolds stress tensor in terms of the mean variables, such as the mean velocity $\bar{u}$.
The simplest closure technique for the Reynolds stress tensor $\bar{\bar{\tau}}$ is based on the observation that turbulence has an effect like viscosity on the fluid, that is it increases the effective mixing velocity and consequently has the same effect of shear stresses, which are proportional to the gradients of mean velocity. Made this consideration, one can derive an expression of the Reynolds tensor analogous to the Newtonian one of the viscous stress tensor exactly because turbulent effects are like viscosity ones. In other words, the turbulent field introduces a sort of virtual diffusivity that mixes the flow. This hypothesis is called Boussinesq hypothesis (Wilcox, 2006), and defines the tensor $\bar{\bar{\tau}}$ in the following way:

$$\bar{\bar{\tau}} = \mu_T(\nabla\bar{u} + \nabla\bar{u}^T) - \frac{2}{3}\rho\, k\, I \qquad (13)$$

where μ_T is the turbulent viscosity and k is the turbulent kinetic energy:

$$k = \frac{[\,(u'^1)^2 + (u'^2)^2 + (u'^3)^2]}{2} \tag{14}$$

Once $\bar{\bar{\tau}}$ is substituted in the averaged Navier–Stokes equations, one obtains:

$$\rho \frac{\partial \bar{u}}{\partial t} + \rho\, \bar{u} \cdot \nabla \bar{u} - \nabla \cdot [(\mu + \mu_T)(\nabla \bar{u} + \nabla \bar{u}^T)] + \nabla \bar{p}* = 0 \tag{15}$$

Where $\bar{p}* = \bar{p}_g + \frac{2}{3}\rho\, k$ is the new modified expression of pressure. Since the static mean pressure is typically much larger than the term $\frac{2}{3}\rho\, k$ then the difference between $\bar{p}*$ and $\bar{p}_g$.

From this last expression of the RANS it is well seen that this equation has the same structure of the standard Navier–Stokes equations for an incompressible fluid, but the effective viscosity given by $\mu_{eff} = \mu + \mu_T$ is used. In reality the turbulent viscosity represents a further unknown that must be determined using a constitutive relation. From dimensional analysis it emerges that:

$$\mu_T = \rho\, \hat{V} \hat{L} \tag{16}$$

where ρ is the density assumed constant, $\hat{V}$ is the turbulent velocity scale that describes the intensity of fluctuations and $\hat{L}$ is the turbulent length scale, related to the dimensions of the largest vortices containing more energy.

The local values of $\hat{V}$ and $\hat{L}$ must be determined using algebraic models or based on $m \in \{0,1,2\}$transport equations, called m-equation turbulence model.
The models of interest in this text are those with two additional differential transport equations, that is the k-ε model, the k-ω model and the SST which is a hybrid between the first two. The two-equation models, differently from those with 0 or 1 equation, allow to completely close the problem without specifying other parameters of the considered flow. Specifically:

- k-ε model: It is one of the most popular turbulence models based on turbulent viscosity and is widely used for its simplicity and efficiency in fully turbulent flows (Launder and Spalding, 1974). Here, k is the turbulent kinetic energy, that represents the energy contained in the turbulent fluctuations of the flow. Instead, ε is the turbulence dissipation, that represents the rate at which turbulent energy is dissipated into heat through viscosity. In this model two transport equations are added, one for k and one for ε, that contain empirical coefficients. These relations are closed and complete, because expressed as function of the other parameters of the problem. Once the two equations are solved, finally, the turbulent viscosity is calculated as:

$$\mu_T = C_\mu \frac{k^2}{\varepsilon} \tag{17}$$

where C_μ is an empirical constant that usually is equal to 0.09.
This model is simple, robust and quite accurate for a wide range of applications. However, it is a model valid for high Re and cannot be integrated up to the wall, that is it would require appropriate modifications for the inner region of the turbulent boundary layer.
The limitations of the k-ε model are that it is not suitable for flows with strong pressure gradients, high vortical component and large curvature of the streamline;

moreover, in regions with high strain rate, the production of turbulent kinetic energy is excessive and therefore not physical, with consequent errors in the model.

- k-ω model: The k-ω model is another formulation that, like the k-ε, solves two transport equations (Wilcox, 2006). However, instead of ε, it uses the variable ω, measured in s^{-1}, that represents the specific dissipation frequency of turbulence, that is it measures the turbulence dissipation per unit of turbulent kinetic energy. In particular:

$$\omega = \frac{\varepsilon}{k} \rightarrow \mu_T \approx \frac{k}{\omega} \tag{18}$$

The k-ω model therefore introduces two transport equations, one for k and one for ω, that allow to close the problem. It has the advantage of being particularly suitable to simulate flows with high pressure gradients and flow separation, therefore in boundary layer flows and especially it can be integrated up to the wall. The only limitation of the standard k-ω model is that of being excessively sensitive to the value of ω in the free stream, therefore to the conditions far from the walls, differently from the k-ε model.

- Shear Stress Transport (SST) model: It is a hybrid model between the k-ε model and the k-ω model, designed to combine the strengths of each one (Menter, 1994). It uses the k-ω model near the walls, where it is more accurate, and the k-ε model in the free stream, where it is more stable.

The SST model introduces a blending mechanism to gradually pass from the k-ω model near the walls to the k-ε model far from the walls, thus ensuring greater accuracy and stability in a wide spectrum of flow conditions. It introduces, moreover, also a correction to limit the production of turbulent viscosity in regions with large velocity gradients, improving the turbulence prediction in these areas. The transport equations used for this model are very similar to those of the k-ω, but with additional

terms that bring the modifications just cited. In the same way as in the k-ω model, also here the turbulent viscosity is calculated as:

$$\mu_T = \frac{k}{\omega} \tag{19}$$

This model is widely used to simulate high-speed aerodynamic flows and for situations with high pressure gradients. Thanks to its capability to manage both the conditions near the walls and the free stream, it is one of the most reliable and stable models in CFD.

2.3 Mesh Generation and Numerical Discretisation

The discretisation of the computational domain represents a fundamental step in the numerical modelling process, as it directly affects both the accuracy and stability of the solution. In the present study, the domain is discretised using the finite element method (FEM), which subdivides the geometry into a set of interconnected elements. Given the geometric complexity of confined indoor environments, unstructured tetrahedral meshes are initially employed to ensure flexibility in representing irregular domains. However, mesh refinement is selectively applied in regions characterised by strong gradients, such as near inlet vents, solid boundaries, and zones of expected flow separation.

Boundary layer regions require careful resolution due to the presence of steep velocity gradients. For this reason, prism or layered elements are introduced close to walls to accurately capture near-wall behaviour.

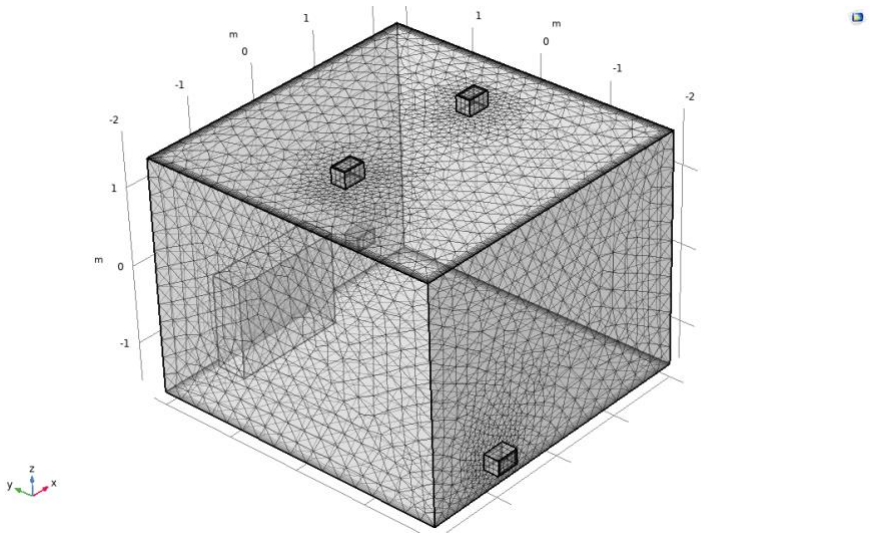

Figure 4. Example of an automatically generated mesh

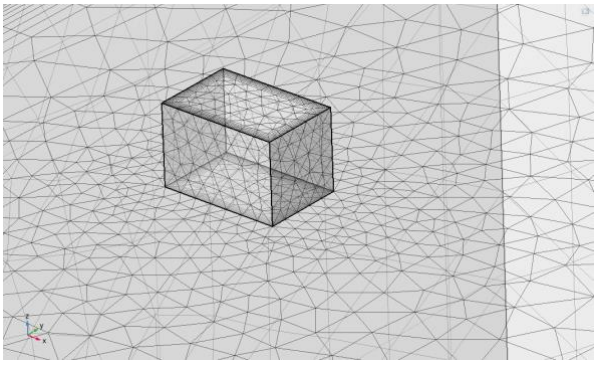

Figure 5. Tetrahedral mesh inlet detail

A key parameter in assessing mesh adequacy for scalar transport is the Péclet number:

$$Pe_e = \frac{Uh}{(2\,D_{eff})} \tag{20}$$

High values of the Péclet number indicate convection-dominated transport, which may lead to numerical instabilities if the mesh is too coarse. In such cases, insufficient resolution may introduce artificial numerical diffusion, smoothing concentration gradients and reducing physical accuracy.

To ensure the reliability of the results, a grid independence study is performed. This consists of progressively refining the mesh and monitoring variations in key output quantities, such as velocity profiles and concentration fields. Convergence is achieved when further refinement produces negligible changes in the solution.
The governing equations are discretised using the finite element formulation. Within each element, the solution variables are approximated using interpolation functions:

$$\varphi(x,t) \approx \Sigma\, N_{i(x)\varphi_{i(t)}} \tag{21}$$

The weak form of the governing equations is obtained through a variational approach (Zienkiewicz and Taylor, 2009), leading to a system of algebraic equations that can be expressed in matrix form:

$$M\frac{dX}{dt} + K(X) = F \tag{22}$$

Non-linearities arising from convective terms are resolved iteratively, typically using Newton–Raphson methods (Ferziger & Perić, 1996). For transient simulations, implicit time integration schemes, such as the Backward Differentiation Formula (BDF), are adopted to ensure numerical stability in convection-dominated regimes.

2.4 Vapour Transport and Removal Modelling

The transport of hydrogen peroxide vapour within the computational domain is modelled using a convection–diffusion equation, coupled with the airflow solution obtained from the CFD model (Bird, Stewart & Lightfoot 1961). In this framework, the vapour is treated as a passive scalar, meaning that its transport is governed by the velocity field without feedback on the momentum equations.
The governing transport equation can be expressed as:

$$\frac{\partial t}{\partial c} + \nabla \cdot (uc) = \nabla \cdot (D\nabla c) + R \qquad (23)$$

where c represents the vapour concentration, u is the velocity field, and D is the molecular diffusion coefficient.

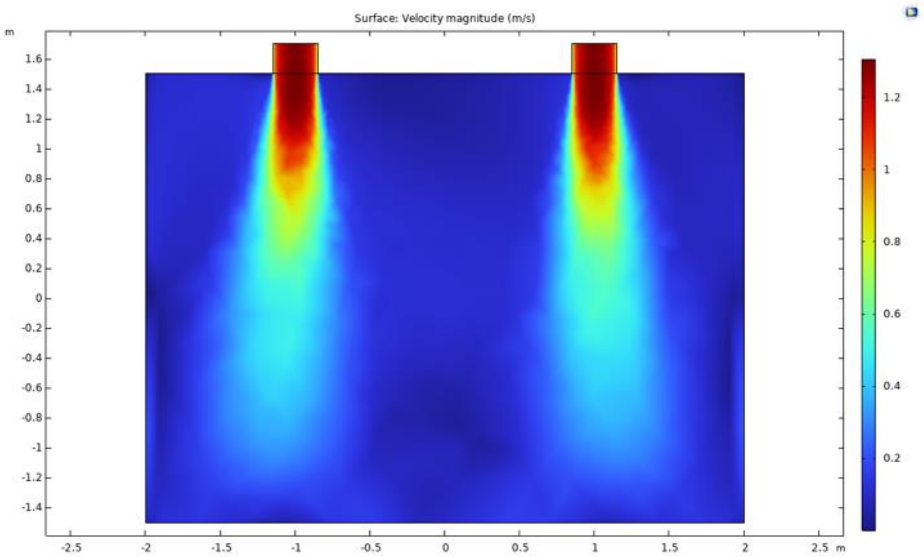

Figure 6. Air ventilation

The transport process is governed by two main mechanisms: convection, driven by airflow, which dominates at large scales; and molecular diffusion, which acts at smaller scales to smooth concentration gradients.

In indoor environments, the relative importance of these mechanisms can be quantified using the Péclet number (Bird et al.). Under typical conditions, high Péclet values indicate that convection is the dominant transport mechanism, implying that the concentration field closely follows the airflow structure.

Boundary conditions play a crucial role in defining the behaviour of the system. At the inlet boundaries, a prescribed velocity field is imposed together with a fixed vapour concentration during the injection phase. At the outlet boundaries, pressure conditions are applied to allow natural flow development. Solid walls are modelled

using no-slip conditions for velocity and zero normal flux for the scalar field, assuming no surface reaction.

The sanitisation process is simulated as a transient phenomenon, capturing both the distribution and removal phases. During the injection phase, vapour concentration increases as hydrogen peroxide is introduced into the domain. During the aeration phase, the concentration decays as a result of ventilation-driven removal.

Safe re-entry conditions are defined conservatively by ensuring that the maximum local concentration falls below prescribed exposure limits, rather than relying solely on volume-averaged values (Chen, 2009). This approach reflects the importance of spatial variability in assessing safety.

The numerical simulations are performed using COMSOL Multiphysics®, which allows coupling between fluid flow and species transport within a unified framework. The modelling workflow includes geometry definition, mesh generation, physics specification, solver configuration, and post-processing of results.

Chapter 3

3.1 Numerical Modelling Strategy

The numerical investigation presented in this study represents the operational implementation of the theoretical framework described in Chapter 2, applied to the analysis of hydrogen peroxide vapour behaviour in confined indoor environments. The modelling approach is designed to capture the key physical processes governing sanitisation, namely airflow dynamics, vapour transport, and concentration decay during aeration. In this context, the numerical model acts as a bridge between theoretical fluid dynamics and practical sanitisation applications.

The airflow within the domain is assumed to be fully turbulent, consistent with the Reynolds numbers associated with mechanically ventilated indoor environments. Hydrogen peroxide vapour is modelled as a passive scalar, implying that its transport is governed by advection and diffusion without influencing the momentum equations (Chen, 2009).

This assumption is justified by the relatively low concentration of vapour compared to the carrier fluid, air, allowing the decoupling of scalar transport from the flow field. Furthermore, chemical decomposition effects are neglected over the characteristic time scales of the simulations, enabling a focus on dominant transport mechanisms.

The transport regime is characterised by high Péclet numbers, indicating that convection dominates over molecular diffusion. As a result, the accuracy of the concentration field is strongly dependent on the correct prediction of the velocity field.

For this reason, particular attention is devoted to ensuring numerical stability and physical consistency of the model. This includes accurate representation of boundary conditions, appropriate turbulence modelling, mesh quality and refinement, and verification of mass conservation.

These elements are not treated as independent numerical aspects, but as integral components of a coherent modelling strategy aimed at preserving both numerical robustness and physical fidelity.

3.2 Computational Implementation in COMSOL Multiphysics®

Multiphysics® is a finite element simulation platform (FEM) that allows to analyze and solve complex physical problems. Engineers and scientists use this software to simulate projects, devices and processes in all the fields of engineering, production

and scientific research, in particular structural mechanics, fluid dynamics, electromagnetism, heat transfer and chemistry.

In this paragraph the software and its structure are presented, since all the work carried out and here described has been performed using this software, with particular attention to the computational fluid dynamics section that COMSOL is able to couple with other physics. The main components of the COMSOL desktop environment are the Model Builder, the Application Builder and the Model Manager.

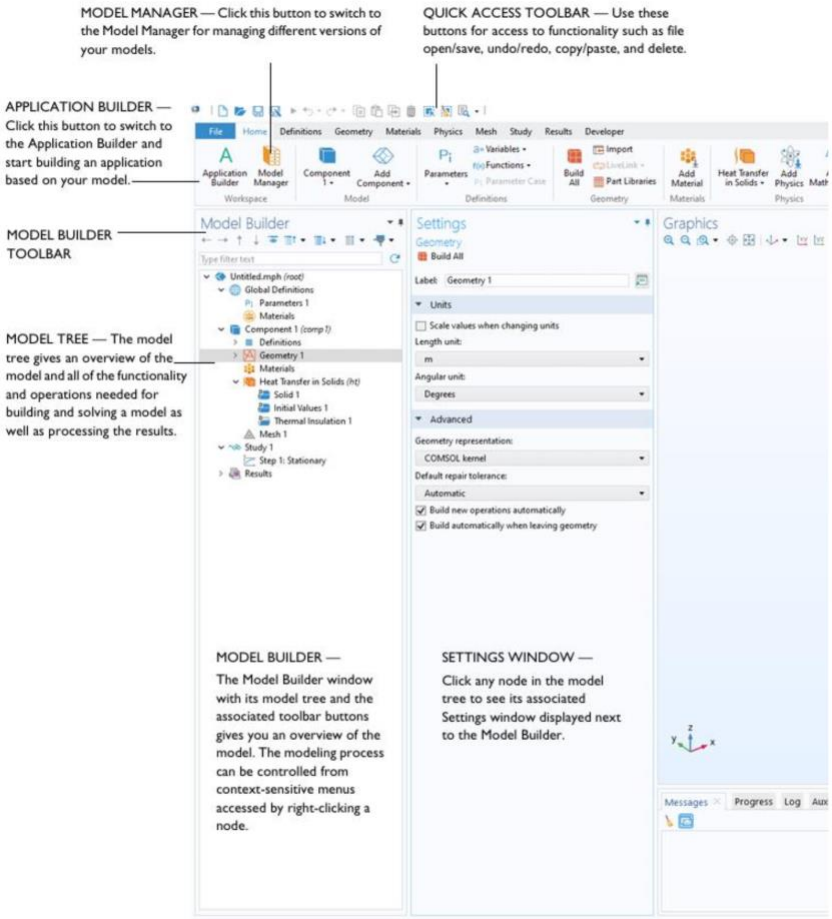

Figure 7. Model builder

The Model Builder is the tool in which it is possible to define the model and its components, for example how to solve it, the analysis of the results and the creation of reports. For this purpose, it is possible to create a model tree. The model tree reflects the structure of the underlying data, that is the model object, which stores the

state of the model, including the settings for geometry, mesh, physics, boundary conditions, studies, solvers, post-processing and visualizations.
The Application Builder allows to quickly create an application (also called app) with a specialized and easy-to-use user interface. An application is generally based on a model created with the model builder.
The Model Manager is a workspace for the management of simulation data that allows to collaborate with other users and centrally organize models and apps. The Model Manager provides version control to keep track of modifications and updates of the files and includes an advanced search tool that allows to search models and applications stored in a Model Manager database for contents based on keywords or tags.
In the Model Builder window each phase of the modeling process, from the definition of global variables to the final report of the results, is visualized in the model tree. One can start with the default model tree, adding nodes and modifying the settings of the nodes. All the nodes of the default model tree are first-level parent nodes. It is possible to right-click on them to visualize a list of child nodes, or subnodes, that it is possible to add under them. This is the means with which nodes are added to the tree. When one clicks on a child node, the node settings are displayed in the Settings window.
From top to bottom, the model tree defines an ordered sequence of operations. In the following branches of the model tree, the order of the nodes makes the difference, and it is possible to modify the sequence of operations by moving the subnodes upward or downward in the model tree.
Before beginning to define the main settings of the simulation, it is necessary first of all to analyze the problem from the physical and analytical point of view. Depending on the dimensions involved and the physics of interest, one will start by setting a problem in 3D choosing between Laminar Flow and Turbulent Flow. After that, one passes to the creation of the working domain.

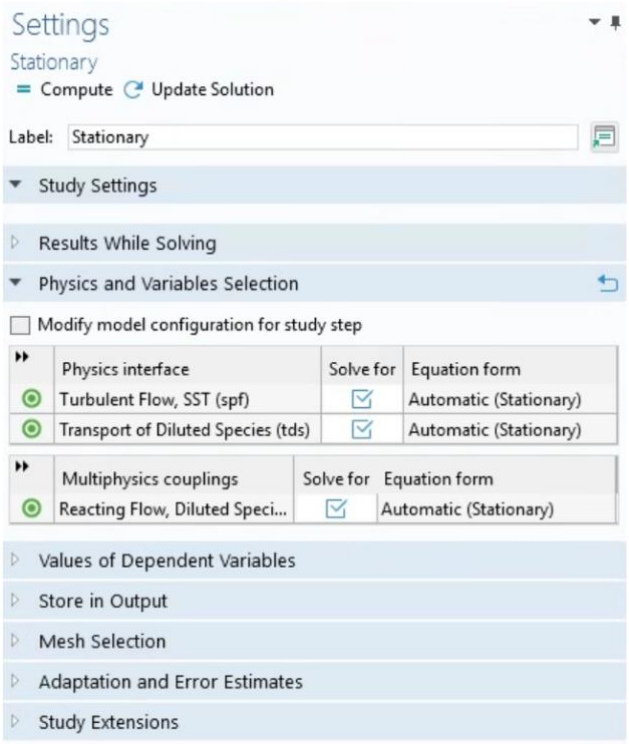

Figure 8. Tab "Study-Stationary"

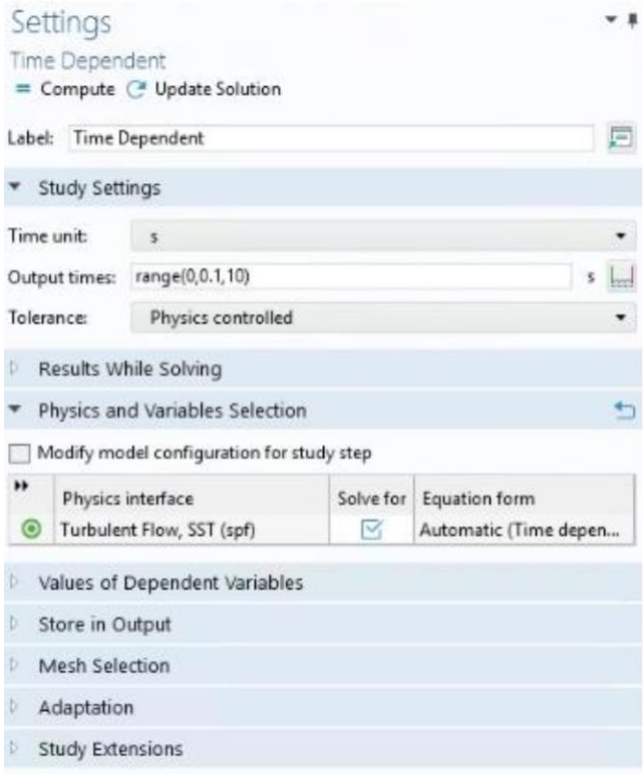

Figure 9. Tab "Study-Time dependent"

The geometry node is the starting point to create and define the geometry of the physical model, in this case of the domain occupied by the fluid. Here it is possible to create, modify or import a two-dimensional or three-dimensional geometry. The domain can be built manually starting from the so-called basic Primitives, such as points, lines, rectangles and squares, circles and ellipses, polygons, blocks, spheres, cylinders and cones. Each of these basic elements can be defined through parameters such as dimensions, position and orientation in space. Moreover, operations can be performed on the generated objects to create more complex geometries. The most important are the Union, which combines multiple objects into a single domain, and the Difference, which subtracts one element from another.

Once the geometry has been created, the next step is the assignment of materials to the model domains, that is to the regions or parts of the geometry. The Materials node is fundamental to define the physical properties of the materials that will be used in the model. These properties directly influence the behaviour of the system and the solution of the physical equations associated to the various simulations.

The Physics node in COMSOL is the heart of the configuration of the physical model and allows to define the equations that describe the behaviour of the system to be simulated. Through this node, it is possible to specify the physical properties, the boundary conditions, the sources and other characteristics that influence the model. COMSOL allows to add multiple physics simultaneously and couple them together. Each physics has a dedicated node under the Physics section, and the variables of one physics can influence other physics, creating coupled models like the one that will be used in this study with CFD and Transport of Diluted Species. An important sub node of the Physics node is the one that allows to set the boundary conditions, fundamental to correctly initialize the problem.

The mesh in COMSOL Multiphysics is a fundamental step to guarantee accuracy and efficiency in the simulations.

The mesh settings, which can be chosen in the Settings window related to the Mesh node, determine the resolution of the finite element grid used to discretize the model.

As already explained in the previous paragraph, the finite element method divides the model into small elements of geometrically simple shapes, for example tetrahedra. COMSOL Multiphysics provides various tools to generate a mesh, and this process can be done automatically or manually, depending on the complexity of the model and the required precision. Since one is speaking about fluid dynamics, it is necessary to generate an ad hoc mesh knowing the problem from the physical and analytical point of view; only in this way it will be possible to have an accurate numerical solution. In this case, the so-called boundary layer represents a critical region to be analysed, therefore in CFD one must pay attention to the generation of the mesh in the regions close to the walls. COMSOL allows to add Boundary Layer, that is a very fine mesh in proximity of the solid surfaces, which allows to accurately model the high gradients present in these regions, such as those of velocity in laminar or turbulent flows.

The Study node is responsible for the definition and the execution of the simulation. Here the necessary steps to solve the numerical model are configured, such as the selection of the appropriate study types (stationary, transient, modal, etc.), the definition of the physical variables and the type of solver used.

When a new study node is generated, COMSOL allows to choose the type of simulation to perform. The options that concern us are: Stationary, for problems that do not depend on time, such as constant laminar flow; Time Dependent, for transient problems in which one wants to study the trend of a flow, for example turbulent, in its temporal evolution.

Each type of study can have different associated solvers. Depending on the complexity of the problem, COMSOL uses numerical methods to solve the equations, such as linear or non-linear solvers, that take care of iterating toward the solution. The Solver Configuration node in the Study node allows to configure the advanced settings for the solver (for example, tolerance, maximum number of iterations, discretization method, etc.).

The Results node allows to visualize, analyse and interpret the results obtained from the simulation. After the Study node has completed the solution of the problem, the calculated data are sent to the Results node for the analysis.
COMSOL offers different types of graphical representations for the simulation results:

- 2D and 3D Plot: They visualize quantities such as temperature, flow velocity, pressure field, etc., through colour maps or surfaces in two or three dimensions.
- Surface plot: Used to visualize scalar variables (e.g. temperature or pressure) on the surfaces.
- Arrow plot: Shows vector fields (e.g. fluid velocity or electric force) as arrows.
- Streamline plot: Visualizes the flow lines to visually represent the direction and the intensity of the fluid flow.
- Contour plot: Represents isolines (or isolevel surfaces) of a quantity, such as contours of constant temperature.
- Slice plot: Allows to visualize a section through a 3D domain.

In addition to graphical representations, the Results node allows to define customized expressions to visualize derived or combined quantities (for example, combining velocity and temperature in a single expression).
Moreover, one can use Cut Planes or Slice plots to see how the selected variable varies inside a section through the three-dimensional domain.

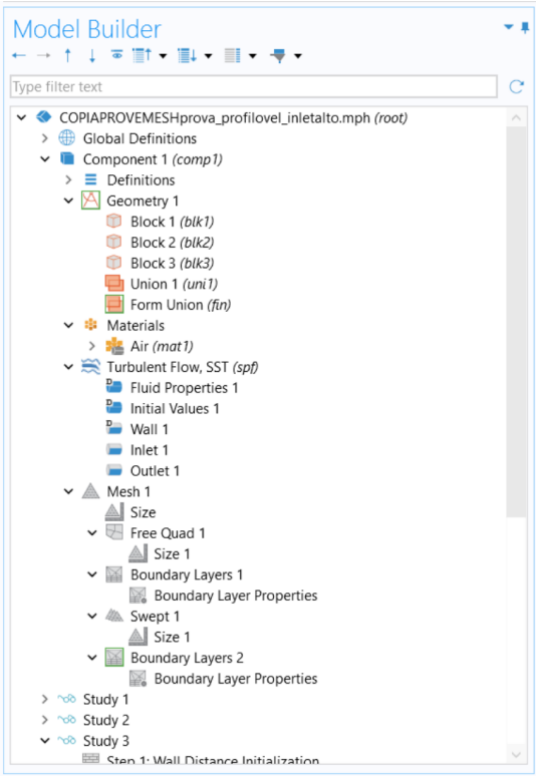

Figure 10. Tree of typical Comsol Simulation

For example, one observes figure 10: it is the tree of a test simulation carried out on the geometry of an empty room, where an air flow entering from a vent placed on the ceiling and exiting in the return vent is considered. To better study the behavior of the fluid in the room, a differentiated mesh has been generated according to the portion of the domain. In fact, on the sections of the square cross-section channel that constitute the inlet and the outlet, a quadrangular mesh has been used, made three-dimensional through the Swept function. In the rest of the domain, the default tetrahedral mesh has been exploited. In proximity of the walls, being a zone characterized by high velocity gradients (boundary layer), the mesh has been refined through the Boundary Layer function.

3.3 Theory of transport of diluted species

The Transport of Diluted Species interface provides a predefined modelling environment for the study of the evolution of chemical species transported by diffusion and convection, as well as migration due to an electric field. The physical interface assumes that all the species present are diluted, that is that their concentration is low with respect to a solvent fluid, in this case air. As a rule, a mixture containing different species can be considered diluted when the concentration of the solvent is higher than 90 mol%. Thus, in this dilution situation, one can assume that the properties of the mixture, such as density and viscosity, correspond to those of the solvent.

The transport of diluted species is governed by the convection–diffusion equation:

$$\frac{\partial c}{\partial t} + \nabla \cdot (-D\,\nabla c + u\,c) = R \qquad (24)$$

where c is the concentration of the species in mol/m³; D is the diffusion coefficient of the species in m²/s; u is the fluid velocity in m/s; R is a term that describes the chemical relations that can consume or produce the species (mol/m³s).

This equation describes the transport of the species by three main processes:

- Molecular diffusion: it is the process by which molecules move from areas with high concentration toward areas with low concentration due to the random thermal motion of particles. It is described by Fick's law:

$$J_d = -D\,\nabla c \qquad (25)$$

where J_d is the diffusive flux of a species; D is the diffusion coefficient, which depends on temperature and fluid viscosity; c is the concentration.
Diffusion is generally the dominant mechanism in systems with very slow or static flows (Bird et al.), or in microscopic systems.

- Convection: In convective transport, the movement of the chemical species is influenced by the movement of the fluid itself. In a fluid moving with velocity u, the species is transported in the direction of the flow. Convective transport is represented by the term u c in the convection–diffusion equation. In many practical cases, convection is the dominant mechanism, especially when the fluid has high velocities or in large systems.

- Chemical reactions: species can be generated or consumed by chemical reactions, described by the term R. It can describe reactions such as decomposition, synthesis, catalytic reactions, adsorption or desorption reactions on surfaces. For example, if species A reacts with species B to form a product P, the reaction rate could be expressed as:

$$R = -k\, c_A c_B \tag{26}$$

where k is the reaction rate constant, c_A and c_B are the concentrations of the reacting species A and B.
When the Transport of Diluted Species module of COMSOL will be used it will be to insert the nebulized hydrogen peroxide into the jet of air entering the conditioned room. In such case what must be specified (Dirichlet boundary condition) will be a known concentration on a surface, for example at the inlet of one or more channels.

The capability of COMSOL to couple the CFD module concerning the fluid flow, in the specific case air, to other physical phenomena, in this case the Transport of Diluted Species module, will be exploited. In such case, the fluid velocity u in the species transport equation can be provided by the fluid dynamics module. The coupling of the CFD part with the Transport of Diluted Species occurs through the convective term $u \cdot \nabla c$, which represents the transport of the species by the fluid flow.

3.4 Geometrical Model and Boundary Conditions

The computational domain represents a confined indoor environment with dimensions of 4 m × 4 m × 3 m, corresponding to a typical room configuration such as a hospital ward, laboratory, or office space.

The geometry includes internal obstacles, such as a cabinet, a desk, and a chair, which are explicitly modelled to account for their influence on airflow patterns. These elements introduce flow separation, recirculation regions, and stagnation zones, which play a critical role in determining vapour distribution.

From a modelling perspective, the inclusion of obstacles is essential to reproduce realistic indoor conditions. Their presence modifies the airflow topology and directly affects both the transport and removal of hydrogen peroxide vapour.

The ventilation system consists of ceiling-mounted inlet vents and corresponding outlet openings. This configuration generates downward airflow jets that interact with the room geometry, producing complex flow structures.

Boundary conditions are defined as follows:

- Inlet boundaries

  A prescribed velocity profile is imposed, together with a fixed vapour concentration during the injection phase. The velocity distribution is designed to represent a realistic turbulent profile rather than a uniform inflow condition.

- Outlet boundaries

Pressure conditions are applied, allowing the flow to adjust naturally to the internal pressure field.

- Solid surfaces

  No-slip conditions are imposed for velocity, ensuring that the airflow adheres to walls and obstacles. For scalar transport, a zero normal flux condition is applied.

The velocity profile at the inlet is derived from analytical considerations to reproduce the behaviour of turbulent flow in ducts. This approach ensures that the jet development within the domain is physically consistent and avoids artificial suppression of shear layer formation.

The combined effect of geometry and boundary conditions determines the resulting airflow structure, which in turn governs vapour transport. For this reason, careful definition of these elements is essential for obtaining reliable and physically meaningful simulation results.

The geometric configuration and its spatial arrangement are illustrated in the following figures:

Figure 11. Elements of geometry in COMSOL

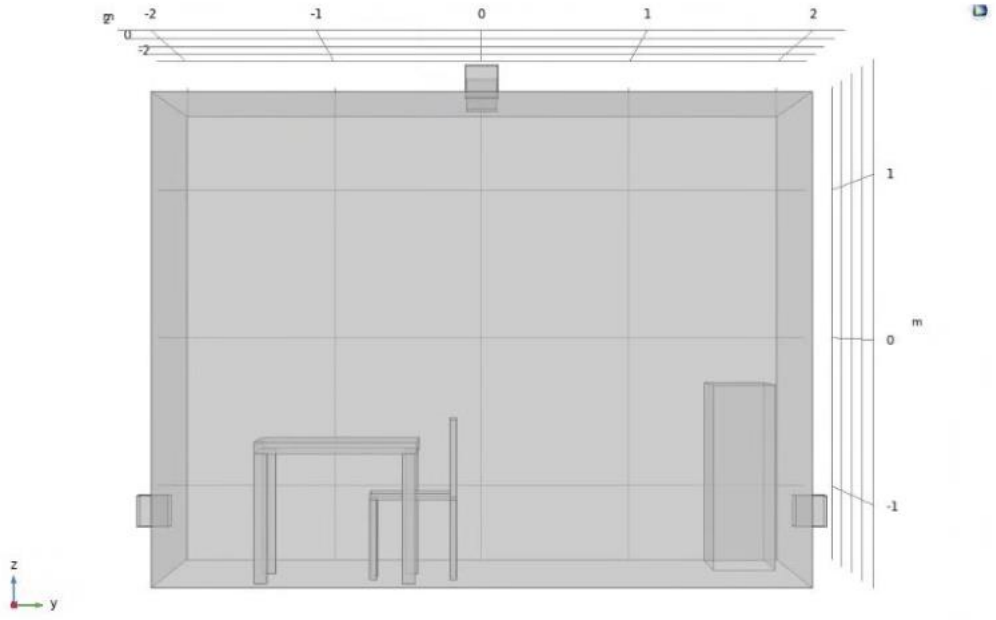

Figure 12. zy plane of the geometry created in COMSOL

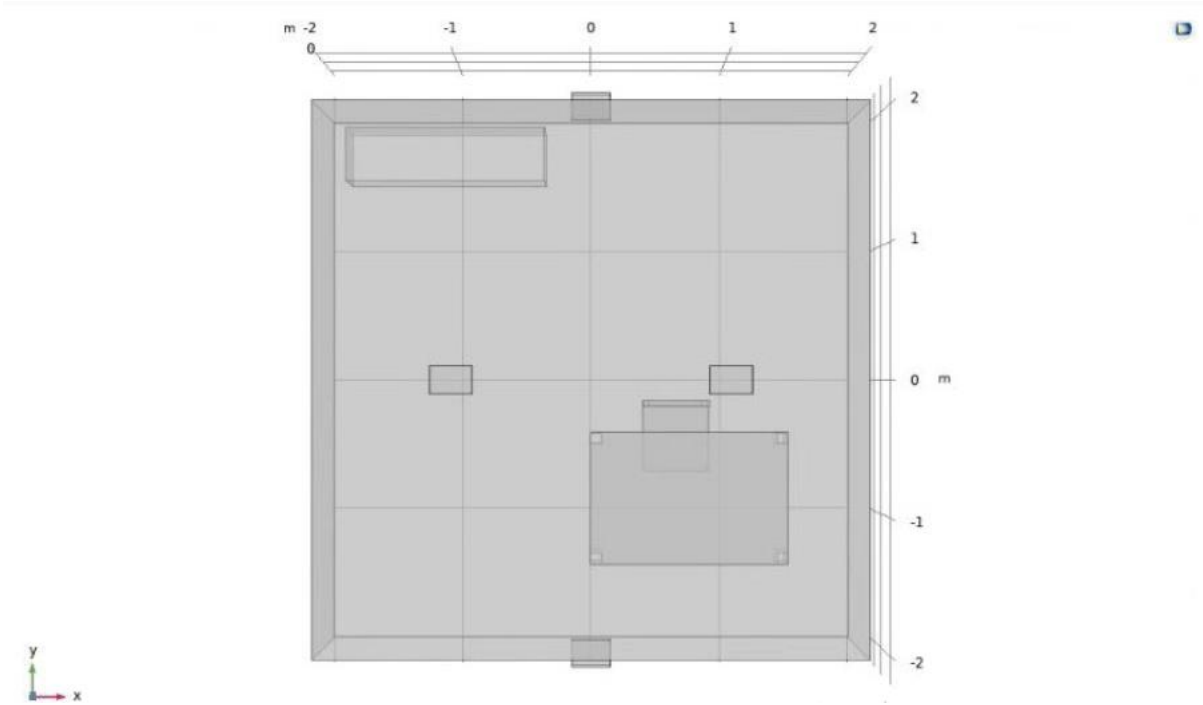

Figure 13. yx plane of the geometry created in COMSOL

These projections clearly display the relative positioning of the supply and outlet vents as well as the distribution of internal obstacles, thereby providing a spatial reference for the interpretation of subsequent flow and vapour distribution results.

3.5 Surface–Vapour Interaction Mechanisms

During vaporised hydrogen peroxide (VHP) decontamination processes, the interaction between the transported vapour and indoor surfaces represents an important aspect influencing both sanitisation effectiveness and post-treatment aeration behaviour. Although the present numerical model primarily focuses on airflow dynamics and species transport within the gaseous phase, surface characteristics may significantly affect local deposition and retention phenomena. From a physical perspective, hydrogen peroxide transport toward solid boundaries is governed by the combined action of convective transport, turbulent diffusion, and near-wall concentration gradients. Once the vapour reaches the surface, its interaction

with the substrate depends on several material properties, including porosity, roughness, permeability, and adsorption capacity.

In the present work, different classes of materials commonly found in confined indoor environments were considered in order to qualitatively analyse their potential influence on hydrogen peroxide retention behaviour. In particular, wooden surfaces, glass materials, and polymeric/plastic substrates were selected due to their significantly different physical characteristics in terms of porosity and surface interaction mechanisms. Wood was considered representative of porous and partially absorbent materials, while glass and plastic surfaces were used to represent smooth and weakly absorbent substrates.

Within the COMSOL Multiphysics environment, material properties were managed through the Material Browser functionality, which allows assignment of physical properties to the computational domains and surfaces involved in the simulations.

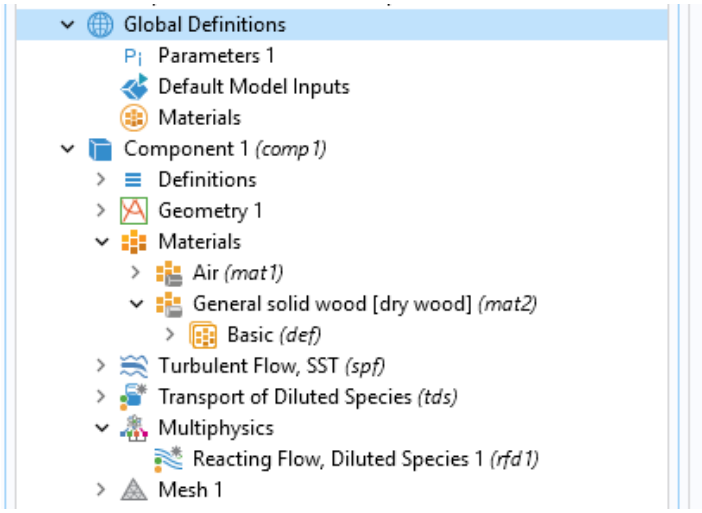

Figure 14. Comsol materials table - wood

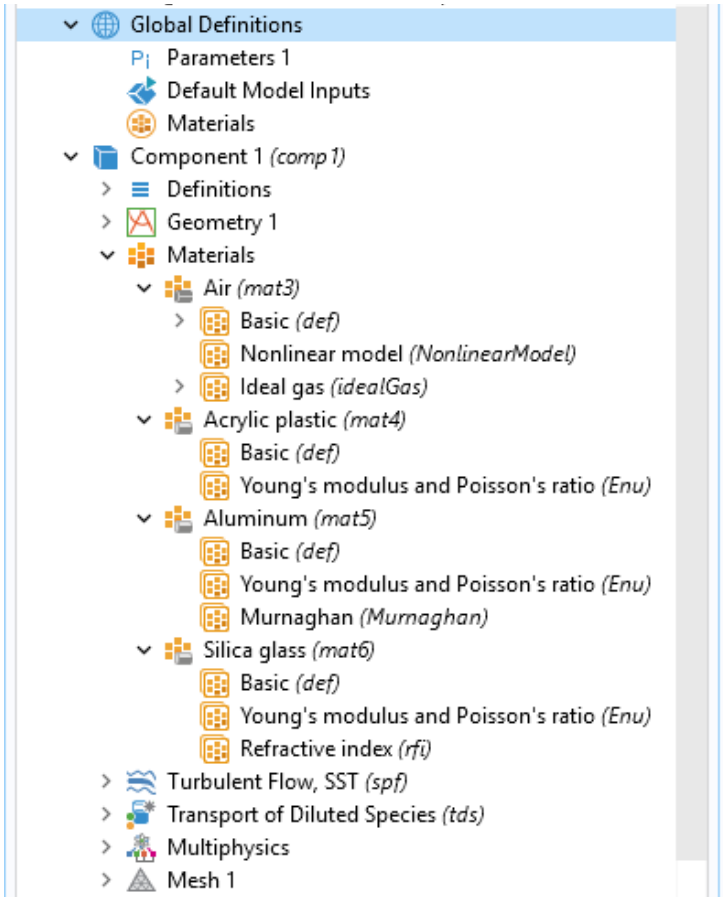

Figure 15. comsol materials table - glass, plastic

Although the present CFD framework did not explicitly implement reactive adsorption or desorption models, the introduction of different material domains enabled qualitative evaluation of the influence of surface characteristics on local airflow behaviour and hydrogen peroxide distribution near the walls.

Porous materials generally exhibit a larger effective surface area due to the presence of microcavities and internal structures capable of promoting local accumulation phenomena. As a consequence, these materials are expected to retain greater quantities of hydrogen peroxide compared to smooth and non-porous surfaces. Conversely, compact materials such as plastics or glass surfaces tend to limit vapour penetration and favour faster desorption processes.

In indoor environments, the fluid dynamic structure of the airflow may further amplify these effects. Regions characterised by low velocity magnitude, recirculation

zones, or weak ventilation conditions may favour prolonged residence times of hydrogen peroxide near surfaces, potentially enhancing local deposition phenomena. On the other hand, highly ventilated regions may promote faster vapour removal and lower local retention.

Although adsorption and desorption mechanisms were not explicitly included in the present CFD framework, the analysis of concentration fields and airflow structures allows qualitative identification of regions potentially associated with enhanced surface retention behaviour. This aspect becomes particularly relevant when considering the restoration of safe environmental conditions after sanitisation, since retained hydrogen peroxide may be progressively released back into the indoor environment during the aeration phase.

Figures 16 and 17 show two representative COMSOL simulations performed at the same exposure time, highlighting the different hydrogen peroxide concentration distributions observed on wooden and glass surfaces.

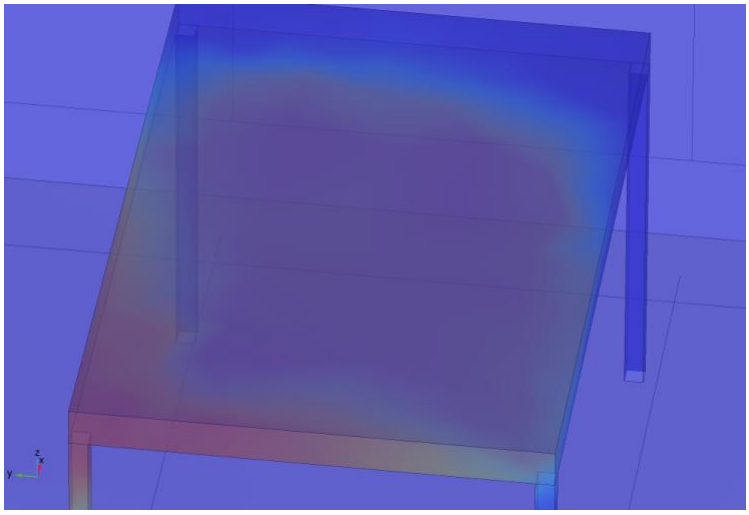

Figure 16. Wood material

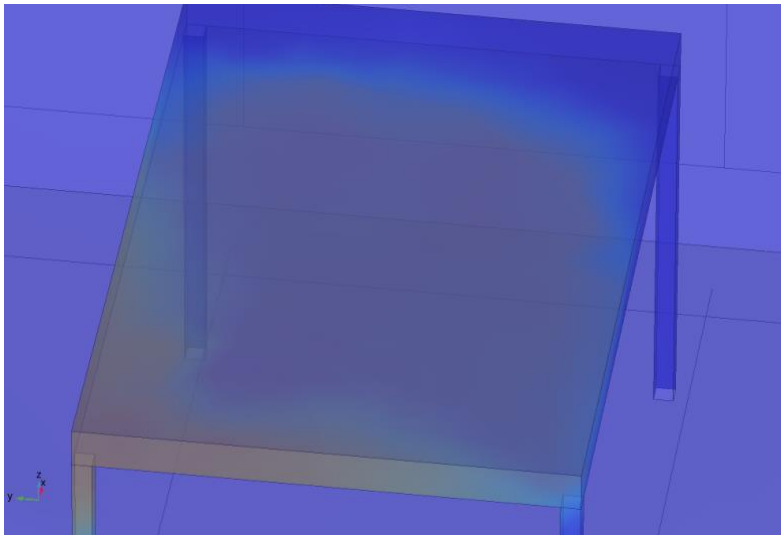

Figure 17. Glass material

The results qualitatively indicate a greater local retention of hydrogen peroxide in correspondence with the wooden substrate, whereas the glass surface exhibits a more uniform and less persistent concentration distribution. These observations are consistent with the different porosity and adsorption characteristics of the analysed materials and further support the importance of surface properties in indoor VHP decontamination processes.

For these reasons, surface–vapour interaction mechanisms should be considered an important factor in the interpretation of VHP distribution within confined environments and represent a relevant future development for advanced CFD-based biodecontamination models.

3.6 Ventilation System and Boundary Conditions

The ventilation system is composed of two rectangular supply vents positioned near the ceiling of the enclosure. Each vent has dimensions of 200 mm × 300 mm, corresponding to an inlet surface area of $S = 0.06\ m^2$. The placement of the supply vents close to the ceiling reflects a typical mechanical ventilation configuration and promotes downward jet development within the room. The outlet vents are arranged symmetrically with respect to the inlet configuration, allowing pressure-driven extraction of air and ensuring a balanced global flow pattern across the domain.

The boundary conditions were defined in a manner consistent with the physical operation of the ventilation system. At the inlet sections, a prescribed velocity field was imposed, derived from the analytical turbulent profile previously discussed. At the outlet boundaries, a reference pressure condition was applied in order to allow the flow to adjust naturally according to the internal pressure distribution generated by the ventilation jets. All walls and solid obstacles were modelled using the no-slip condition, which enforces zero velocity at solid boundaries and ensures that the airflow adheres physically to surfaces.

Within the finite element framework, the no-slip condition is not imposed pointwise but rather in a weak sense through the variational formulation of the governing equations. This approach guarantees mathematical consistency while preserving numerical stability, particularly in regions of strong velocity gradients near solid interfaces.

Since hydrogen peroxide vapour is treated as a passive scalar in the present model, its concentration during the injection phase is imposed as a fixed value at the inlet boundaries. The walls and solid surfaces are considered impermeable, and therefore a zero normal diffusive flux condition is applied. This assumption reflects the absence of reactive surface kinetics within the current modelling scope and ensures that scalar transport remains governed exclusively by advection and molecular diffusion within the fluid domain.

3.7 Derivation and Implementation of the Velocity Profile

A critical aspect of the modelling approach concerns the imposition of a physically realistic turbulent velocity distribution at the inlet vents. Prescribing a uniform velocity profile would artificially suppress shear layer development and distort the natural evolution of the jet inside the enclosure. For this reason, the inlet velocity distribution was derived from analytical considerations applicable to turbulent flow in

rectangular ducts, thereby ensuring consistency between the imposed boundary condition and the expected internal flow behaviour.
The volumetric flow rate is expressed as

$$Q = 0.25WHv_{\mathrm{m}}\left(\frac{\Gamma\left(\frac{1}{2}\right)\Gamma\left(1+\frac{1}{n}\right)}{\Gamma\left(\frac{3}{2}+\frac{1}{n}\right)}\right)^{2} \quad (28)$$

where W represents the vent width, H the vent height, and n is taken equal to 7 in accordance with the empirical formulation for turbulent velocity profiles. From this relationship, the maximum velocity v_max can be determined for a prescribed volumetric flow rate, which in turn is linked to the desired number of air changes per hour.
Once v_{max}own, the spatial velocity distribution across the vent section is defined as

$$v(x,y) = v\_\mathrm{max} - (x/W)^2)\hat{}(1/7)\,(1 - (y/H)^2)\hat{}(1/7) \quad (29)$$

This formulation ensures that the maximum velocity occurs at the geometric centre of the vent while the velocity smoothly decays toward the boundaries. The profile exhibits zero gradient at the centreline and naturally reproduces the shear development characteristic of turbulent duct flows near solid walls. Such behaviour is essential for correctly initiating jet dynamics inside the computational domain.
For example, under a ventilation rate corresponding to eight air changes per hour, the calculated maximum velocity equals

$$v_{max} = 1.0457 \frac{m}{s} \tag{30}$$

The graphical verification of this imposed distribution is illustrated in

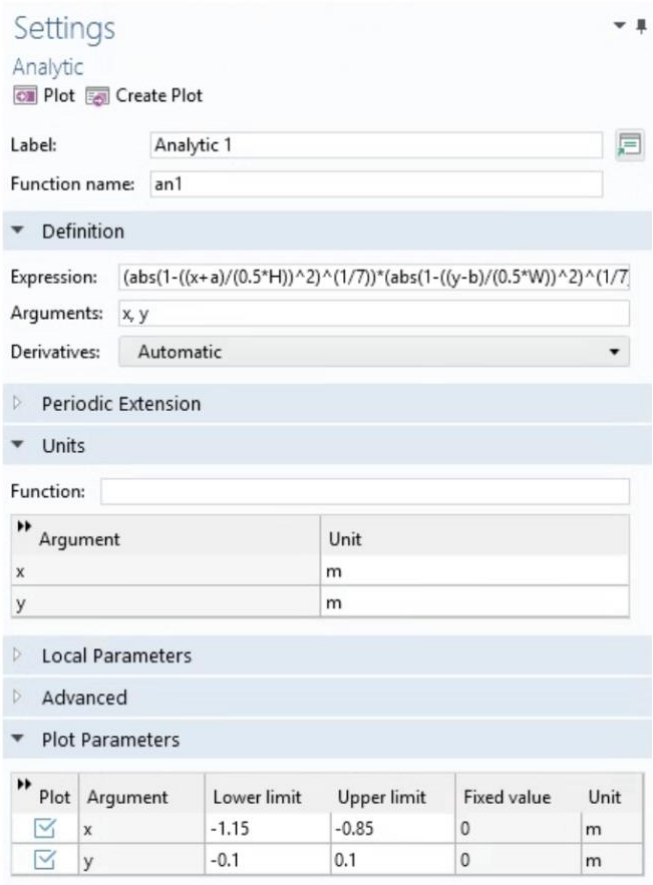

Figure 18. Velocity field function

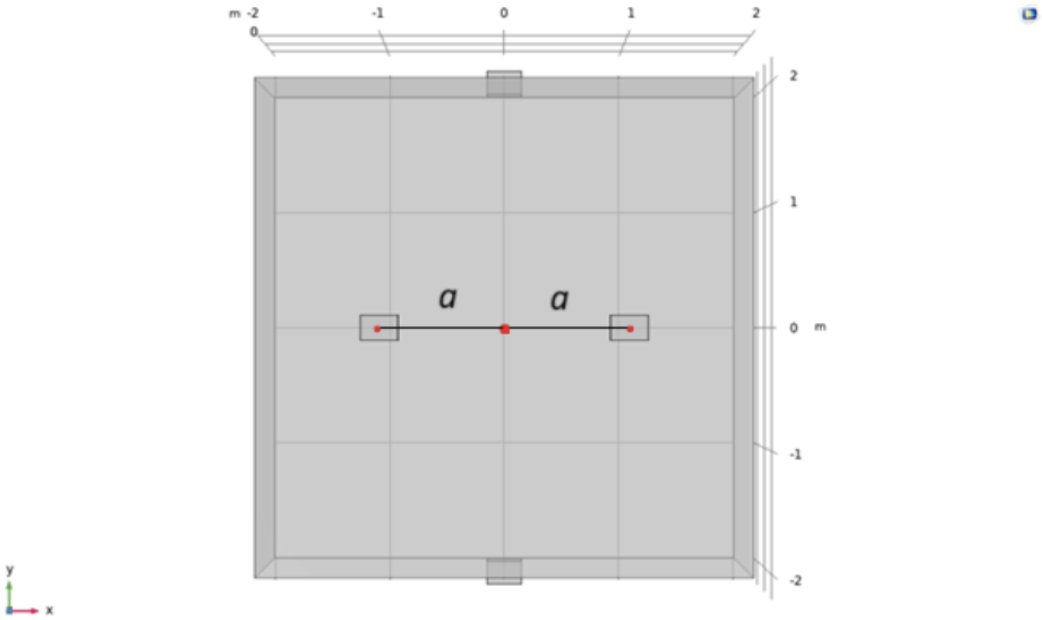

Figure 19. Distances for calculating the velocity field function

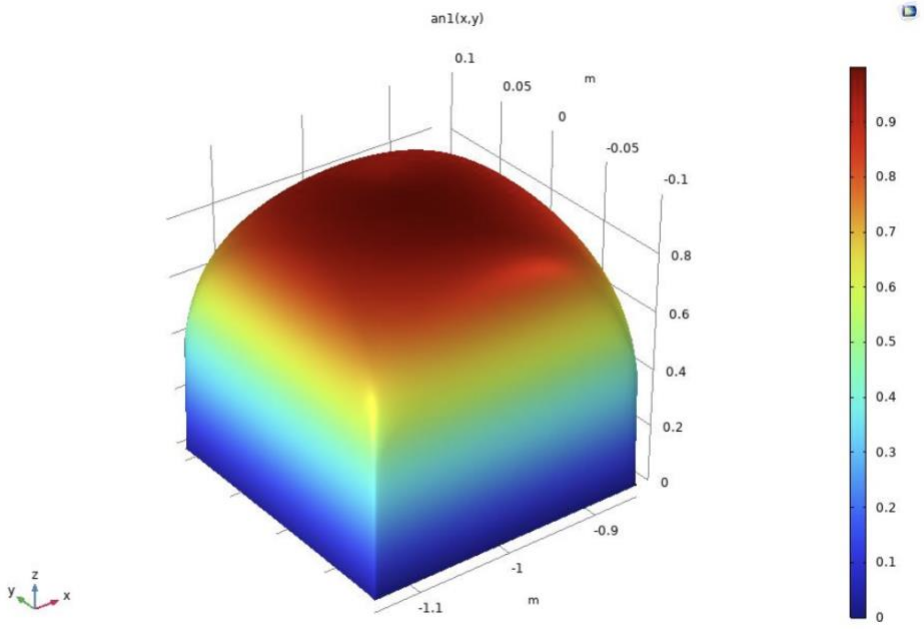

Figure 20. 3D plot of the velocity field function

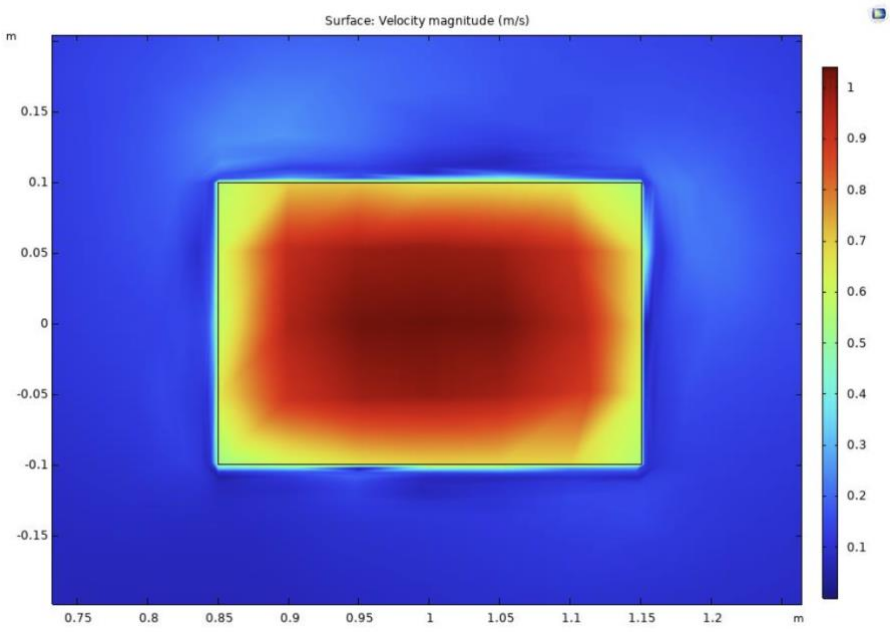

Figure 21. 2D plot of the velocity field on the section of the vent flush with the ceiling

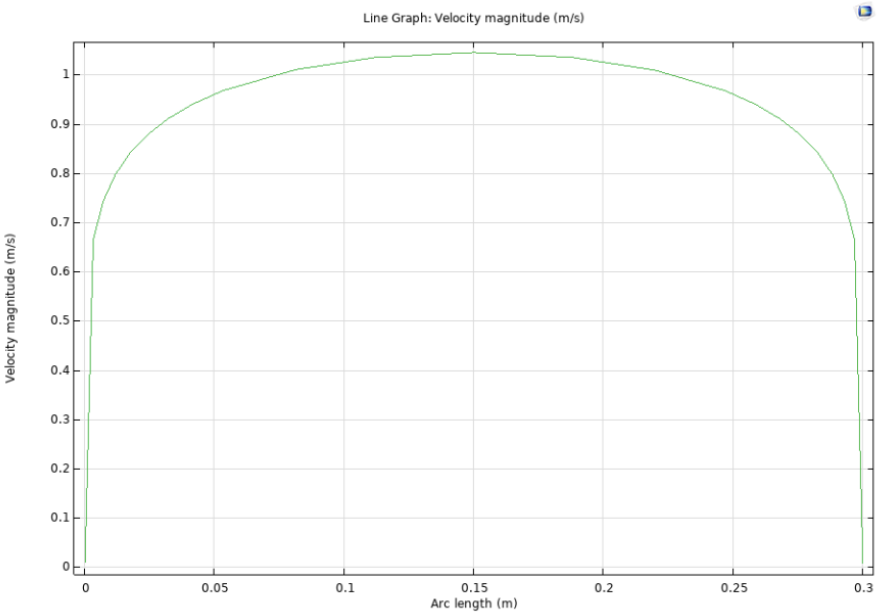

Figure 22. 2D graph of the velocity field function

These representations confirm the expected parabolic-like turbulent profile and demonstrate the coherence between the analytical formulation and its numerical implementation.

It should be noted that, due to the finite element discretisation, the velocity does not strictly reach zero at boundary nodes when coarse meshes are employed. This behaviour arises from the weak imposition of boundary conditions within the variational framework and does not indicate a physical inconsistency. As mesh refinement increases, the approximation improves and the boundary behaviour converges toward the theoretical no-slip condition.

3.8 Governing Equations in Operational Form

The airflow within the computational domain is described by the Reynolds-Averaged Navier–Stokes (RANS) equations, which provide a time-averaged representation of turbulent motion while accounting for the additional stresses generated by velocity fluctuations. The adoption of a RANS framework is justified by the ventilation conditions investigated, as the Reynolds number, defined as

$$Re = \rho \frac{uL}{\mu} \tag{30}$$

confirms a fully turbulent regime for all simulated air change configurations ranging from 2 to 9 ACH (Awbi, 2003). Under these operating conditions, inertial forces dominate viscous effects, and the internal flow structure is characterised by shear layer development, jet impingement, vortex formation and recirculation phenomena. The geometric projections presented in Figures 12 and 13 clarify the spatial arrangement of vents and obstacles that contribute to the generation of such turbulent structures, while the streamline visualisations shown in Figures 35 and 36 illustrate their manifestation within the box.

The transport of hydrogen peroxide vapour is governed by the transient convection–diffusion equation

$$\frac{\partial c}{\partial t} + \nabla \cdot (-D\nabla c + u\, c) = 0 \tag{31}$$

where the first term represents temporal accumulation and the divergence term accounts for the combined effects of advective and diffusive fluxes. The diffusive contribution follows Fick's law and can be expressed as

$$J_d = -D\, \nabla c \tag{32}$$

indicating that molecular diffusion acts in the direction opposite to the concentration gradient. Although diffusion contributes to smoothing concentration differences at small scales, its relative importance must be evaluated in comparison with convective transport.

To quantify this balance, the Péclet number is introduced as

$$Pe = u\frac{L}{D} \tag{33}$$

Using representative values of u ≈ 1 m/s for the characteristic velocity, L ≈ 3 m for the characteristic room dimension, and D ≈ 1.8×10^{-5} m²/s for the molecular diffusion coefficient of hydrogen peroxide in air, the resulting Péclet number is of the order of 10^5. Such a magnitude unequivocally indicates that scalar transport within the enclosure is dominated by advection. In practical terms, this means that the spatial distribution of concentration closely follows the velocity field topology, as evidenced by the alignment between streamline patterns and the corresponding scalar distributions discussed in the section 3.11.

The high Péclet regime therefore reinforces the central methodological requirement of accurately resolving the velocity field. Any numerical inaccuracy affecting shear layers, recirculation zones or jet penetration depth will inevitably propagate into the concentration solution. In convection-dominated environments such as the one analysed, the credibility of hydrogen peroxide distribution predictions depends directly on the fidelity of the computed airflow field.

3.9 Turbulence Modelling Strategy

Given the turbulent regime confirmed by the Reynolds number, the adoption of an appropriate turbulence closure model becomes essential. Direct numerical resolution of all turbulent scales would be computationally prohibitive for the present configuration; therefore, a Reynolds-averaged approach was selected. In this context, the Shear Stress Transport (SST) k–ω model was adopted as the turbulence closure strategy.

The SST formulation represents a hybrid approach that combines the near-wall accuracy of the classical k–ω model with the free-stream robustness of the k–ε formulation. This blending allows the model to retain sensitivity to boundary layer behaviour close to solid surfaces while avoiding excessive dependence on inlet turbulence quantities in the core flow region. Such characteristics are particularly relevant for mechanically ventilated enclosures, where both wall-bounded turbulence and free jet development coexist within the same domain.

From a physical perspective, the ventilation jets entering through the ceiling vents generate complex flow phenomena inside the room (Pope, 2000). As the jets propagate, shear layers develop at the interface between high-momentum core regions and the surrounding air. Upon impingement on opposite walls or interaction with internal obstacles, the flow undergoes separation, giving rise to recirculation bubbles and secondary vortical structures. These features are not merely secondary

details but constitute the dominant mechanisms governing air mixing and scalar transport.

The SST model is especially well suited for predicting flow separation and wall-bounded turbulence, both of which are critical for realistic sanitisation modelling. Accurate representation of these phenomena ensures that recirculation zones, stagnation regions and shear-driven mixing are physically consistent rather than numerically induced artefacts.

Turbulence, in this context, plays a dual role. On the one hand, enhanced turbulent mixing promotes homogenisation of hydrogen peroxide vapour, facilitating more uniform spatial distribution. On the other hand, excessive turbulence intensity may lead to the formation of preferential high-velocity channels that connect inlet and outlet regions directly. In such cases, although global air exchange is accelerated, local exposure times may be reduced in certain parts of the enclosure, potentially affecting sanitisation effectiveness. This balance between mixing enhancement and flow channelisation underscores the importance of carefully modelling turbulence within the CFD framework.

3.10 Finite Element Formulation and Variational Framework

The governing equations introduced previously are solved using the finite element method (FEM). In contrast to finite difference or finite volume approaches, FEM is based on the weak formulation of the governing equations.

Starting from the Reynolds-Averaged Navier–Stokes equations and the scalar transport equation, the solution fields (velocity, pressure, concentration) are approximated through basis functions defined over discretised elements of the computational domain.

The weak form is obtained by multiplying the governing equations by appropriate test functions and integrating over the domain Ω. Integration by parts reduces the order of spatial derivatives, allowing lower-order polynomial interpolation functions.

This formulation ensures:

- Natural incorporation of boundary conditions
- Flexibility in handling complex geometries
- Local refinement capability

However, it also implies that boundary conditions, such as the no-slip wall condition, are imposed in an integral sense rather than pointwise. This explains the slight residual velocity observed at boundaries in coarse meshes.

When $Pe = u\frac{L}{D}$ is very large, as in this study ($Pe \approx 10^5$), convection dominates diffusion. In such cases, classical Galerkin formulation may produce oscillatory solutions (Versteeg and Malalasekera, 2007). COMSOL implements stabilisation techniques (such as streamline diffusion) to mitigate numerical oscillations.

Temporal discretisation for transient simulations is performed using implicit schemes (Backward Differentiation Formula – BDF), which provide unconditional stability for sufficiently smooth solutions.

3.11 Mesh Generation Strategy

The discretisation of the computational domain represents one of the most critical components of the numerical methodology, as it directly influences both the stability of the solution and the physical reliability of the predicted flow structures. In convection-dominated turbulent simulations such as the present case, the quality and distribution of the mesh determine the model's ability to reproduce shear layers, recirculation regions and near-wall gradients without introducing artificial numerical diffusion (Versteeg and Malalasekera, 2007).

The mesh must therefore satisfy multiple and sometimes competing requirements. It needs to resolve the strong velocity gradients that develop in proximity to the inlet jets, where rapid changes in momentum occur over relatively short spatial scales. At the same time, it must accurately capture boundary layer behaviour along solid walls

and obstacles, where velocity decays toward zero under the no-slip condition and scalar gradients may become steep. These local refinements must be achieved without generating an excessive number of elements that would render the computational cost prohibitive. Moreover, element quality must be carefully controlled to avoid excessive skewness or distortion, which could compromise numerical accuracy and convergence behaviour.

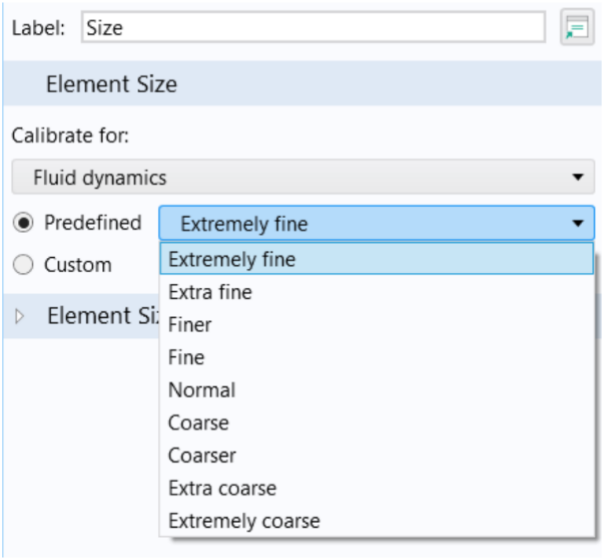

Figure 23. COMSOL predefined mesh sizes

In order to address these challenges in a systematic manner, three distinct mesh strategies were investigated and comparatively evaluated, allowing an informed selection of the discretisation approach that best balances physical fidelity, numerical stability and computational efficiency.

3.11.1 Unstructured Tetrahedral Mesh

The first discretisation strategy adopted in this study consisted of a fully unstructured tetrahedral mesh. As illustrated in figure 24 and figure 25,

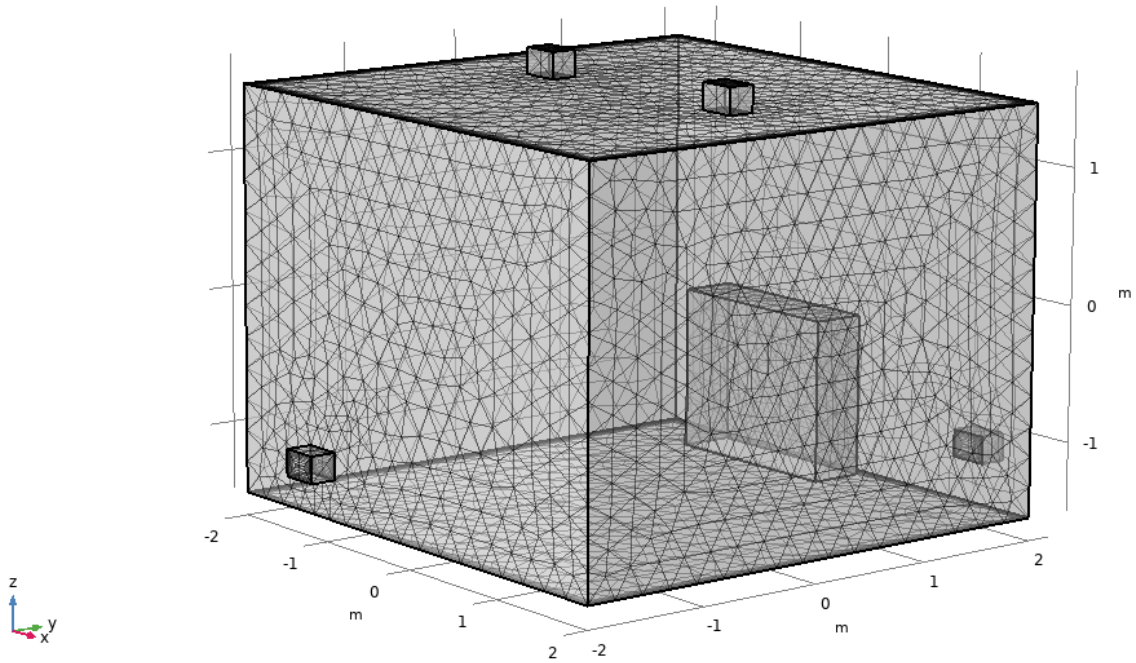

Figure 24. Tetrahedral mesh over the domain

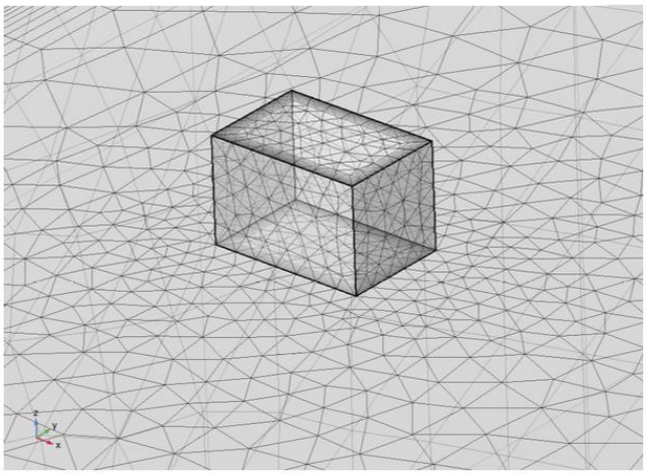

Figure 25. Tetrahedral mesh detail on inlet vent

this approach allows automatic mesh generation and offers considerable flexibility when dealing with geometrically complex domains. The ability of tetrahedral elements to conform to irregular boundaries makes this strategy particularly attractive during the initial stages of model development.

Despite these advantages, the use of fully unstructured tetrahedral elements may introduce numerical diffusion when element quality deteriorates or when gradients are insufficiently resolved. This effect becomes particularly relevant in convection-dominated flows, where artificial smoothing of velocity and concentration fields can alter the physical interpretation of shear layers and recirculation regions.
Initial convergence tests performed with progressive mesh refinement revealed non-monotonic behaviour in the evolution of mass flow rate values. In particular, oscillatory convergence patterns were observed, together with a plateau effect at coarse refinement levels. This plateau can be explained by the geometric constraints imposed by the inlet vents: as long as the characteristic element size remains large relative to the vent dimensions, successive subdivisions do not significantly enhance the resolution of the velocity profile. Only when the element size becomes sufficiently small in comparison with the vent geometry does refinement begin to produce meaningful improvements in the accuracy of the solution. Additionally, the solution proved increasingly sensitive to local element distortion, confirming the strong dependence of numerical stability on mesh quality in unstructured configurations.

3.11.2 Hybrid Mesh: Free Quad + Free Tetrahedral

In order to improve the representation of the boundary regions near the inlet vents, a hybrid discretisation strategy was subsequently implemented. As shown in figure 26,

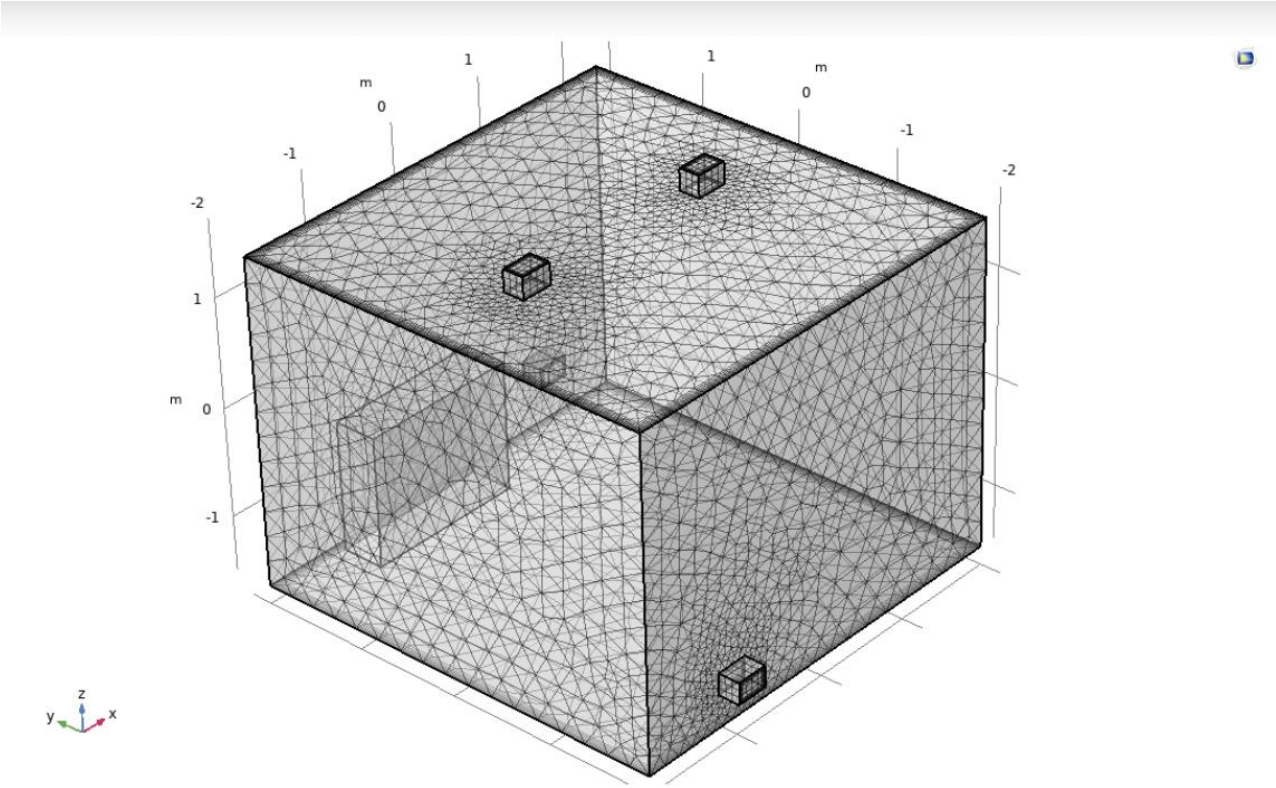

Figure 26. Mesh with Free Quad and Free Tetrahedral

this approach combines different element types within the same computational domain to balance geometric adaptability and numerical accuracy. Quadrilateral elements were applied specifically on the vent surfaces, allowing for a more structured and controlled discretisation of the inlet sections, while tetrahedral elements were used to fill the remaining volume of the domain, preserving flexibility in regions with more complex geometrical features. Additionally, boundary layer elements were introduced adjacent to solid walls, consisting of eight layers with a stretching factor of 1.2, in order to resolve velocity gradients within the near-wall region more accurately.

This hybrid configuration significantly enhances resolution near the inlet sections, where velocity gradients are particularly steep and accurate representation of the imposed profile is essential for realistic jet development. Compared to the fully unstructured tetrahedral mesh, convergence behaviour improves, and the oscillatory patterns observed in earlier tests become less pronounced. Nevertheless, minor oscillations persist at intermediate refinement levels, indicating that while the hybrid

strategy mitigates some of the limitations of the unstructured approach, it does not completely eliminate sensitivity to local discretisation characteristics.

3.11.3 Structured Mapped Mesh

The third and most refined discretisation strategy adopted in this study consists of a user-controlled structured mesh. As illustrated in in the following figures,

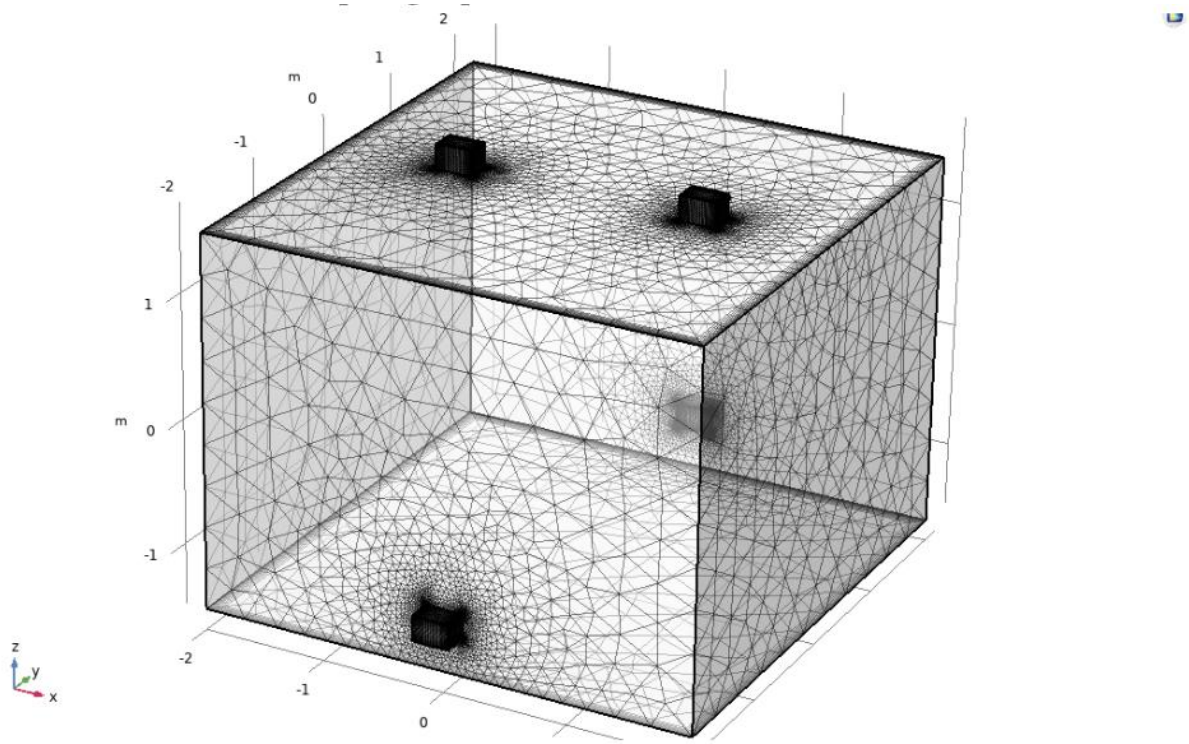

Figure 27. Mapped Mesh and Free Tetrahedral

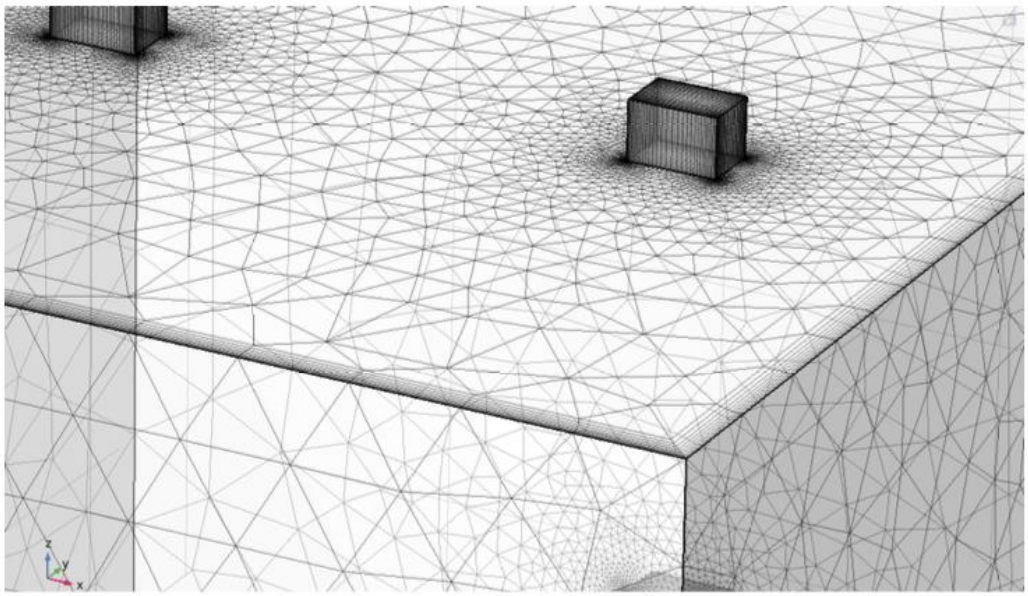

Figure 28. Zoom on vents and Boundary Layers

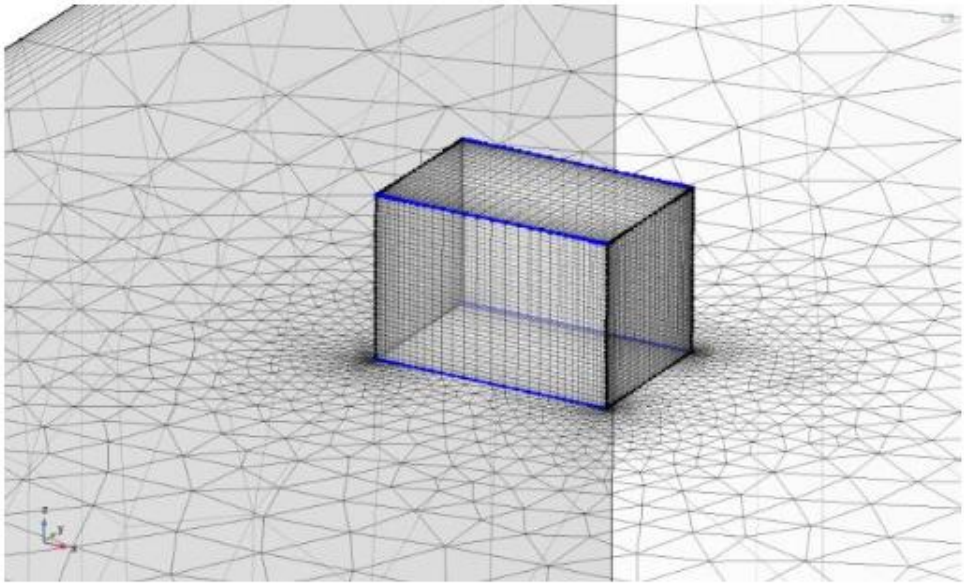

Figure 29. Mapped 1 – Distribution 1

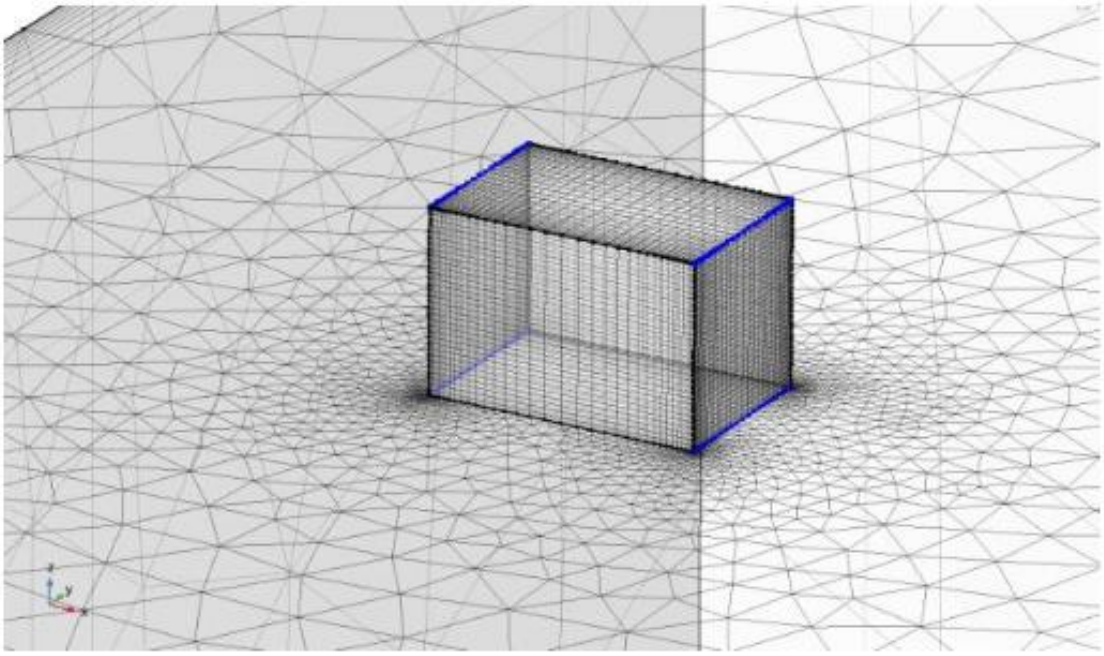

Figure 30. Mapped 1 – Distribution 2

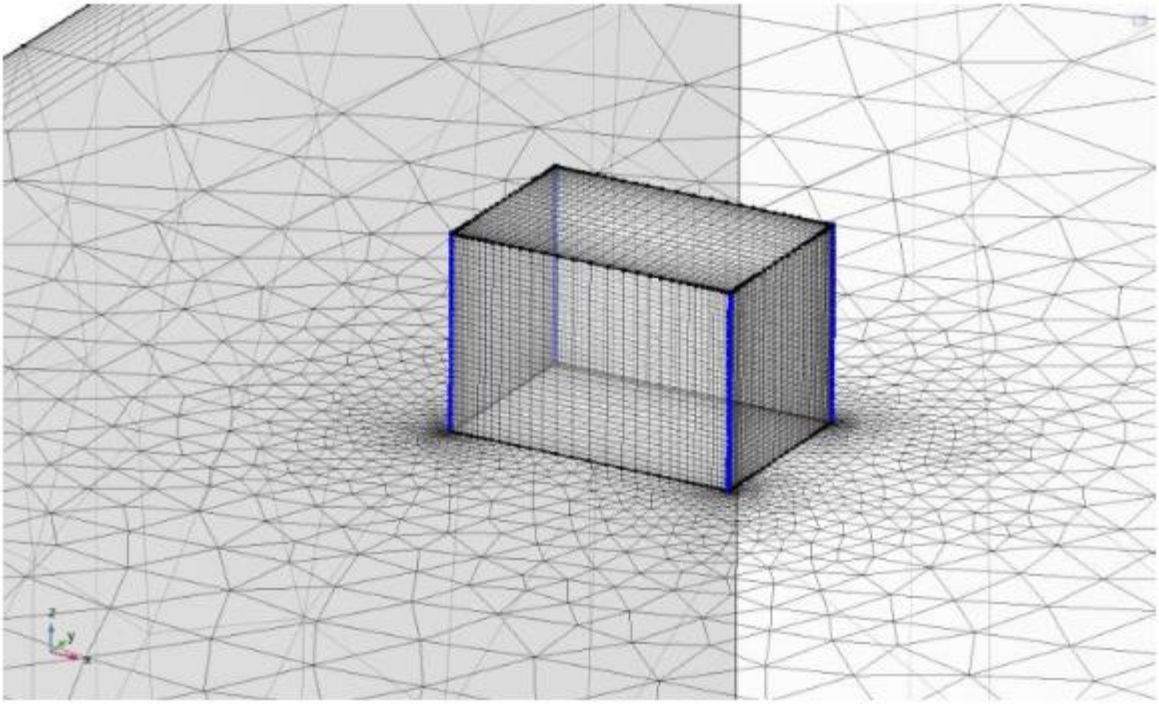

Figure 31. Mapped 2 – Distribution 1

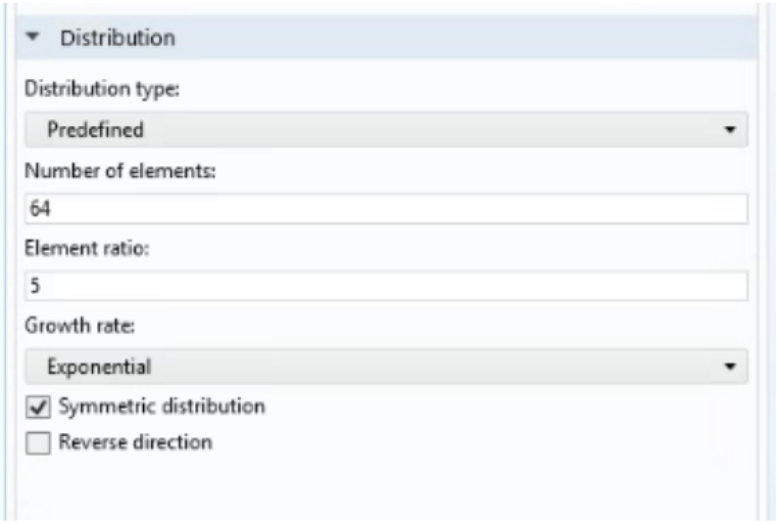

Figure 32. Distribution setting in COMSOL

this configuration introduces a higher degree of control over element placement and refinement compared to the previous approaches.

In this structured configuration, mapped quadrilateral elements are explicitly imposed on the vent faces, ensuring a regular and well-aligned discretisation of the inlet sections where the imposed velocity profile must be accurately represented. The density of elements is regulated through distribution nodes, which allow precise adjustment of the number of divisions along selected edges. Furthermore, the element growth ratio is explicitly prescribed, enabling a controlled variation in element size across the domain. By setting a growth ratio greater than one, a graded mesh is obtained, in which smaller elements are concentrated in regions of high gradients—particularly near walls and vent boundaries—while progressively larger elements are used in regions of smoother flow. This graded approach enhances resolution where it is physically required without unnecessarily increasing the total element count.

The adoption of this structured strategy provides several significant advantages. It enables precise control over the total number of elements and their spatial distribution, thereby optimising computational efficiency. At the same time, it reduces artificial numerical diffusion, preserves the coherence of streamline structures, and promotes monotonic convergence behaviour during refinement

studies. The resulting discretisation not only improves numerical stability but also enhances the physical credibility of the simulated airflow and vapour distribution fields.

3.12 Convergence Assessment

Mesh independence was verified through a systematic refinement procedure, in which the computational grid was progressively refined and the corresponding variation in key global quantities was monitored. The relative difference between successive refinements was quantified using the expression

$$\frac{|P^2 - P^1|}{|P^1|} \tag{34}$$

where P represents either the volumetric flow rate or the mass flow rate evaluated at the outlet boundaries. This metric provides a direct measure of the sensitivity of the solution to discretisation and allows identification of the refinement level beyond which further mesh subdivision produces negligible variation in the computed results.

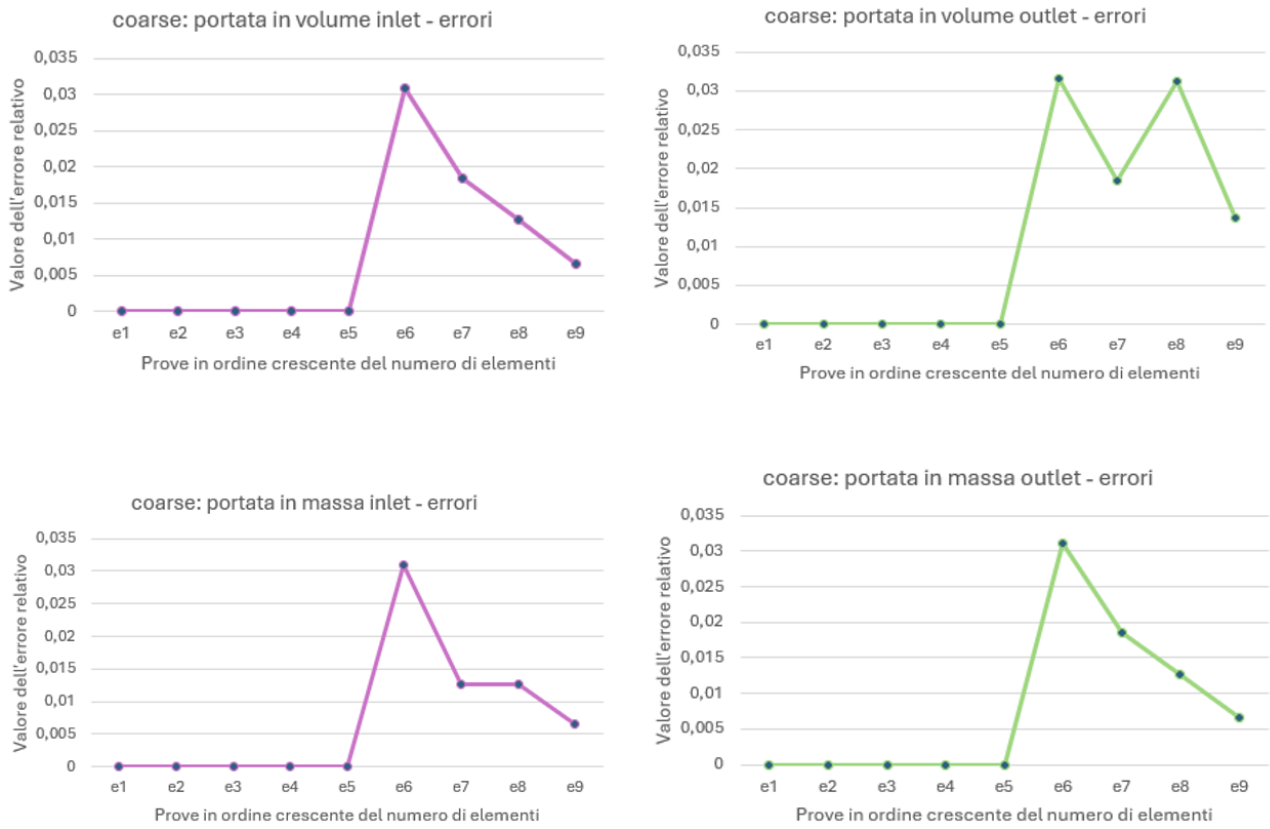

Figure 33. Convergence graph of Coarse Size/Outlet Flow Rate

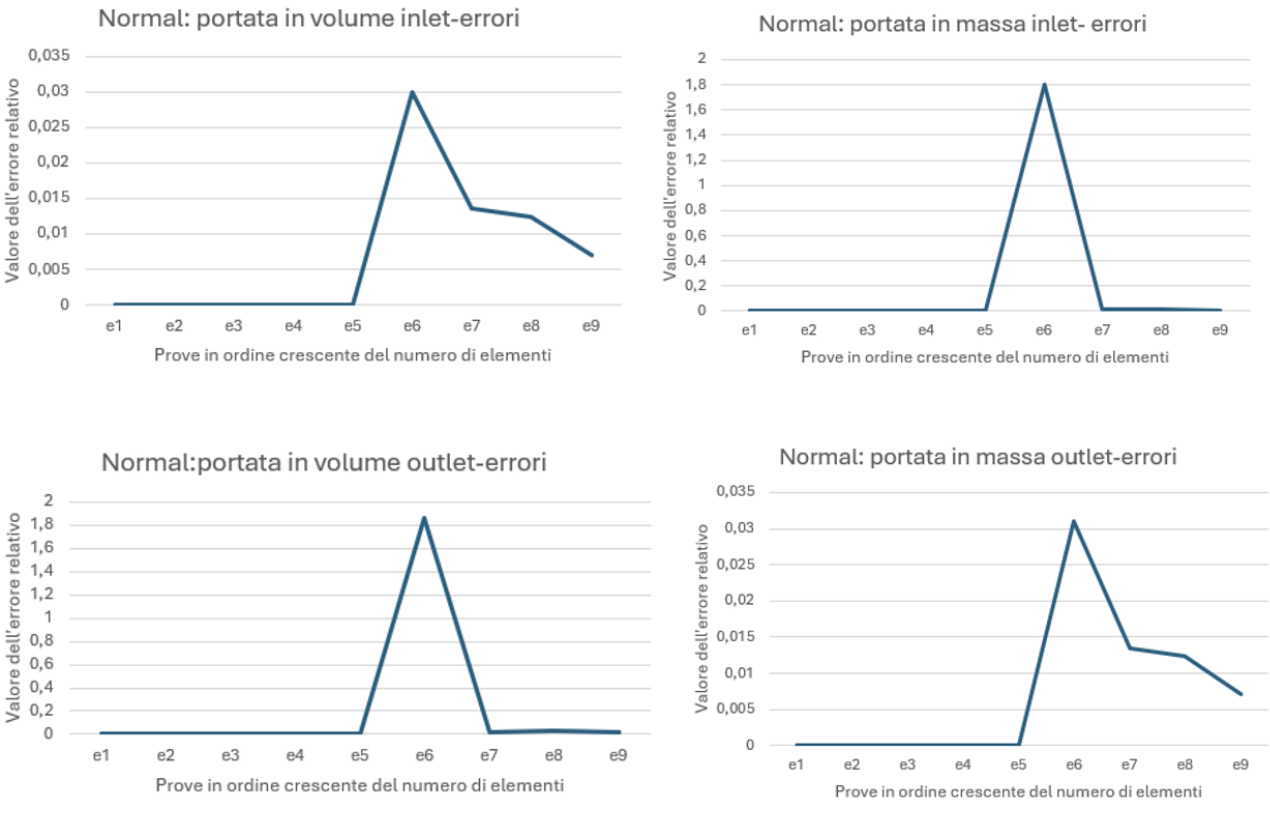

Figure 34. Convergence graph of Normal Size/Outlet Flow Rate

The structured mesh configuration exhibited clear and stable convergence behaviour. In contrast to the unstructured approach, no initial plateau was observed during early refinement stages, and the oscillatory patterns previously detected were substantially reduced. As refinement progressed, the monitored quantities approached an asymptotic value in a monotonic manner, indicating that the solution was no longer significantly influenced by mesh resolution. This behaviour confirms that the discretisation strategy ensures both numerical stability and physical consistency. Additional validation was performed by comparing the numerically evaluated flow rate with the theoretical value derived from the imposed inlet velocity profile, expressed as

$$P_{theoretical} = v \cdot A \tag{35}$$

The relative deviation between theoretical and computed values was calculated as

$$\frac{|P_{theoretical} - P_{evaluated}|}{|P_{theoretical}|} \tag{36}$$

The minimal deviation observed in this comparison confirms the correct implementation of boundary conditions and verifies mass conservation within the computational domain. Together, these tests demonstrate that the adopted mesh configuration provides a reliable basis for subsequent analysis of airflow and vapour distribution.

3.13 Interpretation of Mesh Influence on Flow Structure

The influence of mesh quality becomes particularly evident when analysing the topology of streamlines within the computational domain. A direct comparison between different discretisation strategies reveals how strongly the predicted flow structures depend on the underlying grid resolution and element organisation. This is illustrated in following figures,

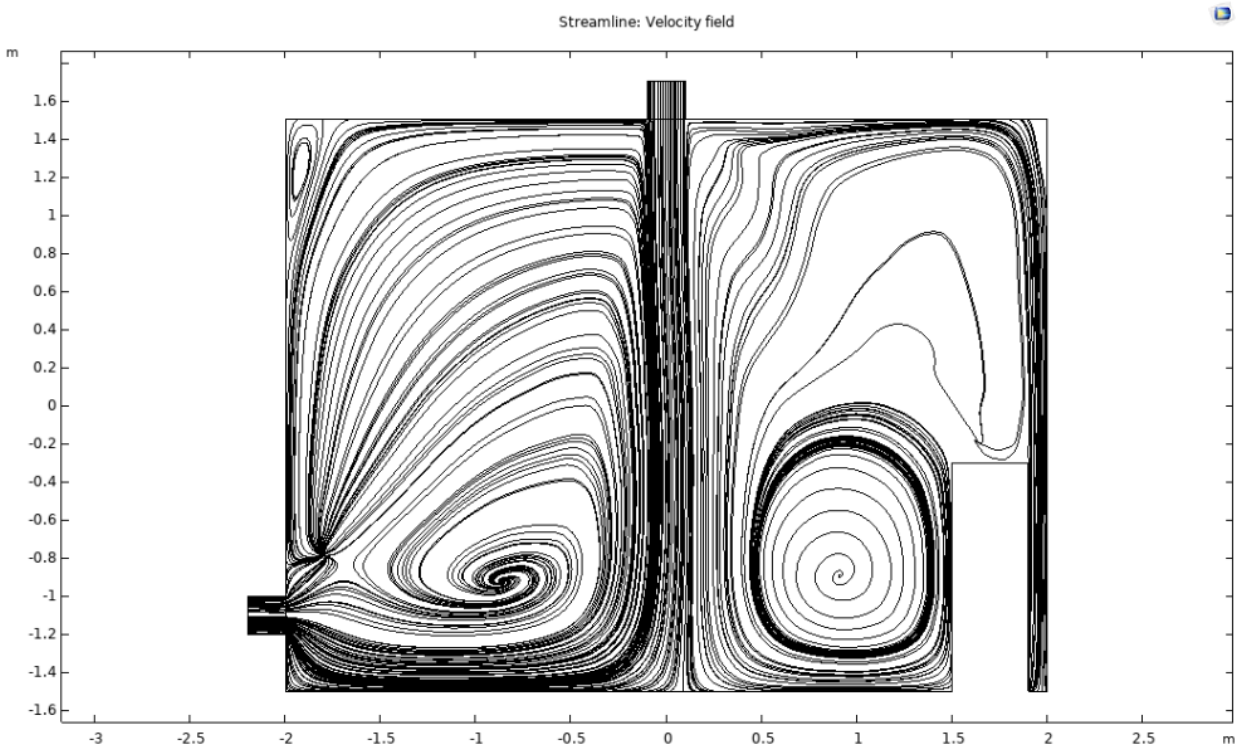

Figure 35. 2D plot of streamlines on a yz plane at x = −1, in the case of a structured mesh

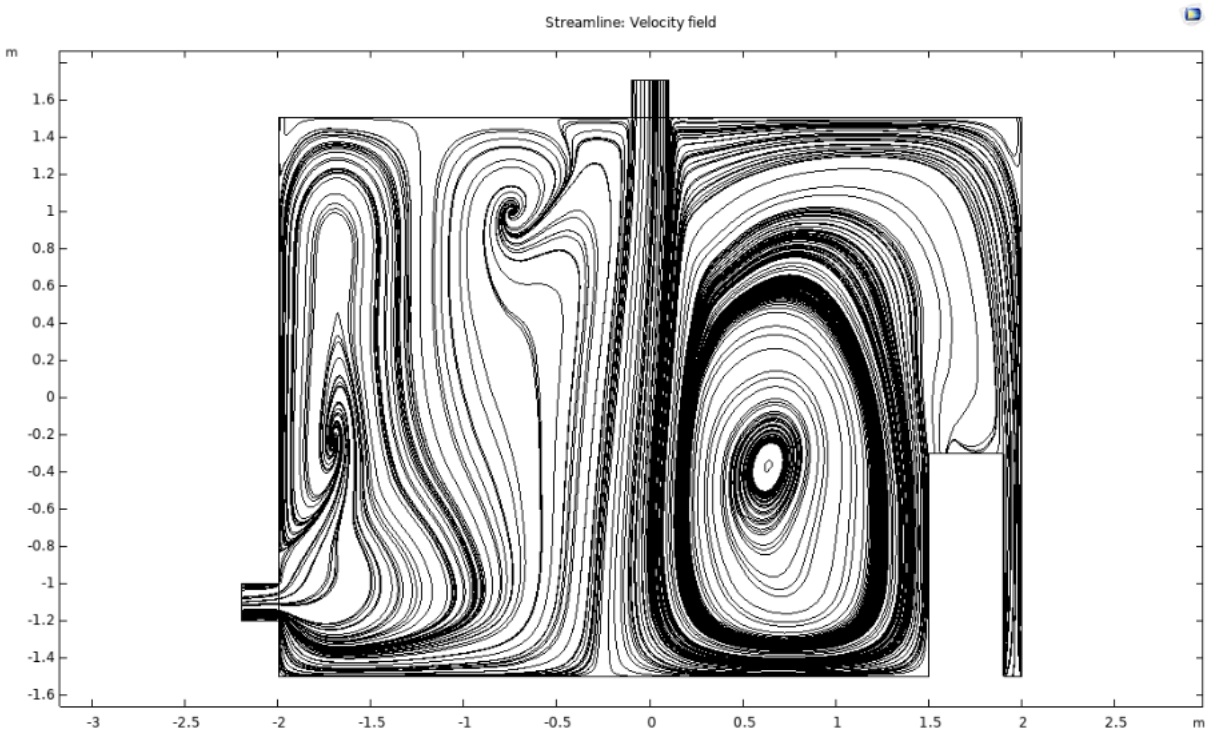

Figure 36. 2D plot of streamlines on a yz plane at x = −1, in the case of an unstructured mesh

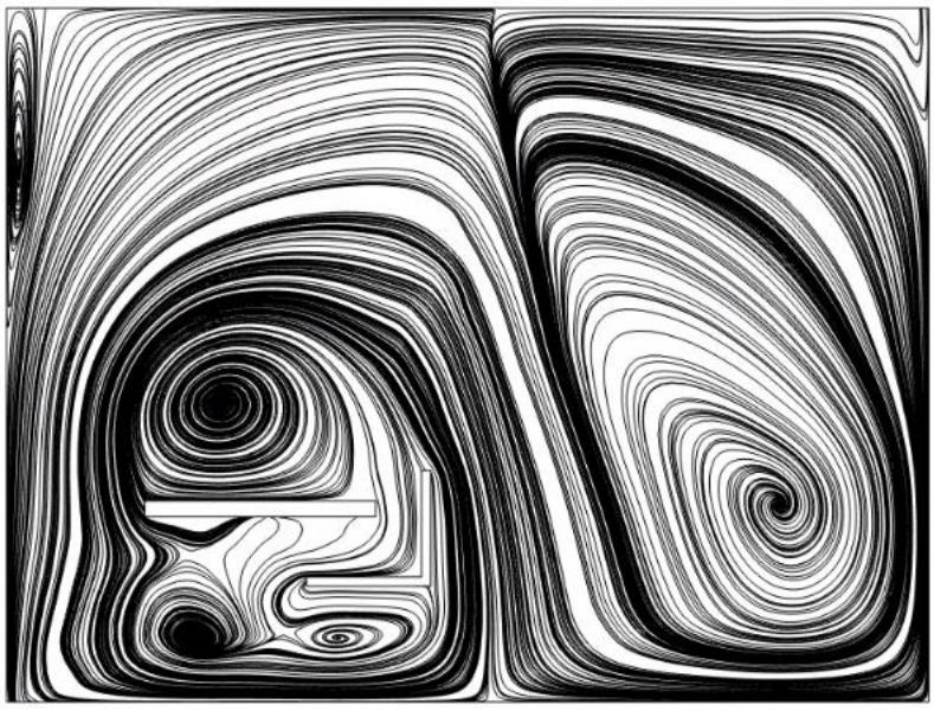

Figure 37. Streamlines behaviour in presence of obstacles, yz plane, Cut Plane at x = 0.7

In the structured mesh configuration, streamlines adhere smoothly to the surfaces of internal obstacles and follow coherent trajectories throughout the domain.

Recirculation regions appear clearly defined and physically plausible, and flow separation near obstacle edges is captured with continuity and geometric consistency. The resulting flow field exhibits well-organised shear layers and stable vortex structures, which are essential for accurately describing mixing and scalar transport. By contrast, the unstructured mesh produces a less consistent representation of the flow. Artificial streamline termination may be observed in certain regions, indicating local numerical artefacts. Velocity gradients are less sharply resolved, and recirculation zones appear diffused or irregular. As a consequence, the overall flow structure seems less physically credible, particularly in areas where sharp changes in direction or velocity magnitude are expected.

This comparison confirms that the reliability of vapour distribution predictions depends directly on mesh quality. Since hydrogen peroxide transport is strongly convection-driven, any distortion in the velocity field inevitably propagates into the concentration field. Accurate discretisation is therefore not merely a numerical refinement, but a prerequisite for physically meaningful interpretation of sanitisation dynamics.

3.14 Air Changes per Hour and Scaling of the Flow Regime

Having established the discretisation strategy and verified mesh independence, the numerical model was subsequently employed to investigate the influence of ventilation rate on the internal flow structure. The principal operational parameter governing mechanical ventilation is the number of air changes per hour (ACH), defined as

$$ACH = Q \cdot \frac{3600}{V} \tag{37}$$

where Q denotes the volumetric flow rate and V represents the total volume of the enclosure (Awbi, 2003).

In the present configuration, the room volume is V = 4 × 4 × 3 = 48 m³. For a prescribed ACH value, the corresponding volumetric flow rate follows directly from

$$Q = ACH \cdot \frac{V}{3600} \tag{38}$$

and the inlet velocity is then consistently obtained from

$$v_{in} = \frac{Q}{n_{vents} \cdot S} \tag{39}$$

where S = 0.06 m² and n_vents = 2. This procedure ensures that the local boundary condition imposed at the inlets is fully coherent with the global ventilation requirement, thereby preserving mass balance and physical consistency across scales. As ACH increases from 2 to 9, inlet velocities increase proportionally. Because velocity appears linearly in the numerator of the Reynolds number expression, the Reynolds number scales linearly with ACH. This scaling is not merely a mathematical consequence but has direct implications for the structure of the turbulent flow inside the enclosure.

At higher Reynolds numbers, inertial forces increasingly dominate viscous effects, promoting the amplification of shear instabilities within the inlet jets. The growth rate of turbulent fluctuations increases, shear layers thicken more rapidly, and energy cascades toward smaller eddies become more pronounced. Jet penetration depth increases accordingly, as the high-momentum core retains coherence over longer distances before diffusing into the surrounding air. These mechanisms collectively enhance turbulent mixing and promote faster redistribution of hydrogen peroxide vapour throughout the domain.

However, the enhancement of turbulence intensity does not translate into a strictly proportional improvement in spatial homogenisation. While increased Reynolds

number strengthens mixing at the scale of shear layers and eddies, it may also reinforce dominant jet structures that establish preferential pathways between inlet and outlet. In such conditions, global air exchange is accelerated, but lateral dispersion can become less effective, particularly in peripheral regions shielded by obstacles. The resulting flow field reflects a complex interplay between turbulence amplification, geometric confinement, and recirculation dynamics.

This non-linear relationship between ventilation rate and homogenisation efficiency underscores the necessity of spatially resolved CFD analysis. The detailed consequences of Reynolds scaling on vapour distribution, recirculation persistence, and exposure uniformity will therefore be examined in depth in Chapter 4.

3.15 Convective Dominance and Scalar Transport Regime

The scalar transport regime within the enclosure is characterised by the Péclet number (eq. 33).

Under typical indoor ventilation conditions, representative values can be assumed as $u \approx 1$ m/s for the characteristic velocity, $L \approx 3$ m for the characteristic length scale of the room, and $D \approx 1.8 \times 10^{-5}$ m²/s for the molecular diffusion coefficient of hydrogen peroxide vapour in air. Substituting these values yields $Pe \approx 10^5$, indicating that advective transport overwhelmingly dominates molecular diffusion. (Bird et al.)

A Péclet number of this magnitude implies that scalar transport is governed primarily by the velocity field, while diffusion contributes only marginally at the scale of the enclosure. As a consequence, the concentration field tends to align closely with the topology of the streamlines. Any distortion or inaccuracy in the computed velocity solution is therefore directly transmitted to the scalar distribution, reinforcing the central role of accurate flow prediction. Under these conditions, mesh quality becomes even more critical, as insufficient spatial resolution may introduce artificial numerical diffusion or oscillatory behaviour in the scalar field. For this reason,

stabilisation techniques embedded within the numerical formulation are essential to prevent non-physical concentration fluctuations in convection-dominated regimes. Because molecular diffusion is comparatively weak, regions that are shielded from the main flow by obstacles or located within recirculation zones may experience delayed exposure to hydrogen peroxide vapour. In such areas, scalar transport relies almost entirely on convective mixing rather than diffusive spreading. This phenomenon is particularly relevant for sanitisation effectiveness, since surface exposure time may vary significantly across the enclosure, leading to spatial heterogeneity in decontamination performance.
The governing transport equation

$$\frac{\partial c}{\partial t} + \nabla \cdot (-D\nabla c + u\, c) = 0 \qquad (40)$$

must therefore be interpreted as strongly advection-dominated, and accurate representation of convective flux becomes essential. In this context, preserving the physical integrity of the velocity field is not simply a computational objective, but a prerequisite for meaningful prediction of hydrogen peroxide vapour distribution.

3.16 Theoretical Concentration Decay and Model Validation

A simplified reference model for a perfectly mixed room assumes that concentration remains spatially uniform throughout the entire volume at any given time. Under this idealised assumption, the temporal evolution of concentration follows the well-known exponential law

$$C(t) = C0\, e^{-ACH\, t} \qquad (41)$$

which derives directly from a global mass balance equation in which instantaneous mixing is presumed. In this formulation, the rate of concentration decay depends exclusively on the ventilation rate expressed in terms of air changes per hour, and no spatial gradients are considered.

In reality, however, confined environments rarely achieve perfect mixing instantaneously. The presence of ventilation jets, internal obstacles and recirculation zones introduces spatial heterogeneity that cannot be captured by a zero-dimensional model. CFD simulations provide the opportunity to quantify the deviation between the idealised exponential decay predicted by the perfectly mixed assumption and the actual transient behaviour resolved in space and time.

Despite its simplicity, the theoretical exponential model remains valuable. It offers a practical means of estimating clearance time, serves as a reference for validating the global consistency of numerical results, and provides a macroscopic description of average concentration behaviour. By comparing the simulated spatially averaged concentration with the analytical exponential decay, it becomes possible to assess whether the numerical model reproduces the expected large-scale mass balance dynamics.

If the spatial average of the simulated concentration follows the exponential trend while local variations remain significant, this indicates that the model successfully captures both global and local aspects of the transport process. In such a case, the CFD framework not only satisfies the overall mass balance but also resolves the spatial structures responsible for concentration heterogeneity, thereby offering a more complete representation of sanitisation dynamics than the idealised well-mixed approach.

3.17 Numerical Stability and Error Propagation

In convection-dominated regimes, discretisation error may propagate along flow direction. The local truncation error in FEM discretisation depends on element size h and polynomial order p, typically scaling as:

$$Error \propto h^p \tag{42}$$

Structured mesh allows systematic reduction of h in regions with high gradient, particularly near inlet jets and wall boundaries.

Residual monitoring ensured convergence of nonlinear solver iterations. Stability of time integration was verified by testing progressively smaller time steps until temporal convergence was achieved.

The implicit BDF scheme provides unconditional stability for linear problems and robust behaviour for nonlinear turbulent systems. Adaptive time stepping allowed balancing computational cost and accuracy.

3.18 Transition Toward Flow Field Analysis

The methodology developed in this chapter ensures geometric fidelity in the representation of the computational domain, physically consistent boundary conditions, an appropriate turbulence modelling strategy, verified mesh independence, numerical stability of the transient solver, and rigorous conservation validation. These components are not independent technical steps but interconnected elements of a unified modelling strategy. Geometric accuracy guarantees that the airflow pathways reflect realistic obstruction effects; consistent boundary conditions ensure physical coherence between imposed ventilation rates and internal flow evolution; turbulence modelling allows reliable prediction of shear layers and

recirculation zones; mesh independence confirms that the numerical solution does not depend on discretisation artefacts; numerical stability prevents artificial oscillations; and conservation validation ensures that mass balance is respected throughout the simulation.

Together, these aspects provide the necessary foundation for interpreting simulation results in a physically meaningful manner. Without such methodological robustness, any analysis of vapour distribution would risk being influenced by numerical artefacts rather than genuine flow physics.

The following chapter therefore shifts the focus from formulation to interpretation. It examines in detail the structure of the flow field, the topology of streamlines, the development of recirculation patterns, and the influence of air changes per hour on mixing efficiency. Particular attention is devoted to the spatial distribution of hydrogen peroxide vapour and to the comparison between the theoretical exponential decay model and the transient behaviour obtained from CFD simulations. This transition from methodology to results is critical, because a reliable numerical framework acquires scientific value only when it enables rigorous interpretation of the underlying physical mechanisms governing sanitisation performance.

Chapter 4

Results and Discussion

4.1 Flow Field Structure and General Behaviour

The numerical methodology developed in Chapter 3 provides the foundation for a detailed and physically grounded interpretation of the airflow structure inside the

mechanically ventilated enclosure (Pope, 2000). The purpose of the present chapter is not merely to report numerical values or graphical outputs, but to analyse the resulting velocity and concentration fields in terms of the underlying fluid dynamic mechanisms that govern vapour distribution.

As established in Chapter 2, the airflow behaviour is controlled by a turbulent regime characterised by the Reynolds number.

For all ventilation configurations investigated, the calculated Reynolds numbers confirm fully turbulent conditions. Under such circumstances, inertial forces dominate viscous effects, leading to the development of shear layers, the formation of vortical structures, and the emergence of recirculation regions throughout the enclosure (Pope, 2000).

When air enters the domain through the rectangular ceiling-mounted vents, two primary jet structures develop. These jets initially preserve a high-momentum core and propagate downward before spreading laterally because of entrainment and interaction with the surrounding air. As they impinge on opposite walls and encounter internal obstacles, their trajectories are deflected and complex flow structures emerge. Although the boundary conditions are geometrically symmetric, the resulting flow field does not remain perfectly symmetric. This asymmetry arises from the inherently nonlinear nature of turbulence, combined with the geometric perturbations introduced by the presence of furniture and other obstacles within the domain.

The coherence of these structures can be observed in the figure 35.

In this configuration, streamlines exhibit smooth and continuous trajectories, reflecting a physically consistent development of the inlet jets. The jets maintain significant momentum near the ceiling region and progressively diffuse as turbulent mixing increases. Recirculation zones form downstream of obstacles, particularly in the vicinity of the cabinet and beneath the desk, where flow separation occurs and vortical patterns stabilise.

A contrasting representation is provided by figure 36. In this case, insufficient mesh resolution compromises the coherence of streamline topology. Artificial streamline termination and local discontinuities become evident, revealing the influence of discretisation quality on the predicted flow structures. These numerical artefacts do not merely affect graphical appearance but may distort the interpretation of mixing and scalar transport.

The comparison between structured and unstructured discretisation thus demonstrates that numerical methodology directly influences physical interpretation. In a convection-dominated regime, where concentration fields closely follow velocity structures, the credibility of vapour distribution analysis depends fundamentally on the reliability of the computed airflow field.

4.2 Jet Penetration and Recirculation Structures

The inlet jets exhibit the characteristic behaviour of turbulent wall-bounded jets. Immediately downstream of the vents, the velocity profile retains a pronounced high-momentum core, which preserves its coherence over a finite distance before progressively diffusing into the surrounding air. At the interface between the jet and the ambient fluid, shear layers develop as a result of velocity gradients, giving rise to enhanced turbulent mixing. These shear layers represent regions of intense momentum exchange and play a central role in redistributing both kinetic energy and scalar concentration throughout the enclosure.

As the jets propagate further into the domain, they eventually impinge on the opposite wall or interact with internal obstacles. At this stage, flow separation occurs and the organised kinetic energy of the jet is partially transformed into turbulent fluctuations and recirculation bubbles. The redistribution of energy from mean flow to turbulence contributes to the formation of complex vortical structures that persist in the vicinity of solid surfaces.

This behaviour is clearly illustrated in figure 37, where the formation of recirculation zones behind the cabinet becomes evident. These regions are particularly relevant from a sanitisation perspective, as the convective transport of hydrogen peroxide vapour is significantly reduced within them. In such zones, airflow velocities are lower and mixing is governed predominantly by local turbulent fluctuations rather than by direct jet penetration.

From the standpoint of hydrogen peroxide distribution, these recirculation structures represent potential areas of delayed exposure. The high-momentum jets primarily dominate the central regions of the enclosure, where advective transport is strongest, while low-velocity recirculating flow characterises shadowed regions shielded by obstacles. Mixing between these two regimes occurs mainly along the shear layers that separate the jet core from the surrounding fluid.

Because the scalar transport regime is characterised by $Pe = u\,L / D \gg 1$, concentration fields closely follow these velocity structures. In a convection-dominated environment, the organisation of the flow field directly determines the spatial distribution of vapour, reinforcing the importance of accurately resolving jet dynamics and recirculation behaviour for realistic assessment of sanitisation performance.

4.3 Influence of Air Changes per Hour on Flow Dynamics

Increasing the air changes per hour modifies the global flow regime in a manner that is predictable from a dimensional standpoint, yet not strictly linear in its physical consequences. Since the Reynolds number scales proportionally with ventilation rate according to the general equation and velocity increases directly with ACH, one might initially expect a monotonic improvement in mixing as ventilation intensity rises. The simulations, however, reveal a more articulated behaviour.

At relatively low ACH values, typically between 2 and 3, the inlet jets possess limited momentum and therefore exhibit reduced penetration depth. The high-momentum core dissipates more rapidly, and large recirculation regions tend to occupy substantial portions of the enclosure. These extended vortical structures are clearly visible in the streamline representations derived from the geometrical configuration illustrated in figures 12 and 13 and further evidenced in figure 37. Under such low-ventilation conditions, mixing proceeds more slowly and the global residence time of air parcels remains comparatively long. While this may favour prolonged exposure locally, it also delays the achievement of homogeneous vapour distribution.

As ACH increases toward intermediate values, typically in the range of 5 to 6, the flow structure undergoes a qualitative transition. Jet penetration becomes more pronounced, shear layers intensify, and turbulent kinetic energy increases sufficiently to disrupt previously persistent stagnant zones. The recirculation bubbles that dominate low-ACH configurations shrink in spatial extent, as shown in the comparative flow fields presented in the velocity plots, particularly those corresponding to refined mesh conditions (figures 35 and 36). In this intermediate regime, mixing efficiency improves markedly, and coverage uniformity across surfaces becomes more consistent. The concentration field, while still influenced by geometry, displays reduced large-scale heterogeneity.

At high ACH values, between 8 and 10, the situation becomes more complex, as shown in the following figures.

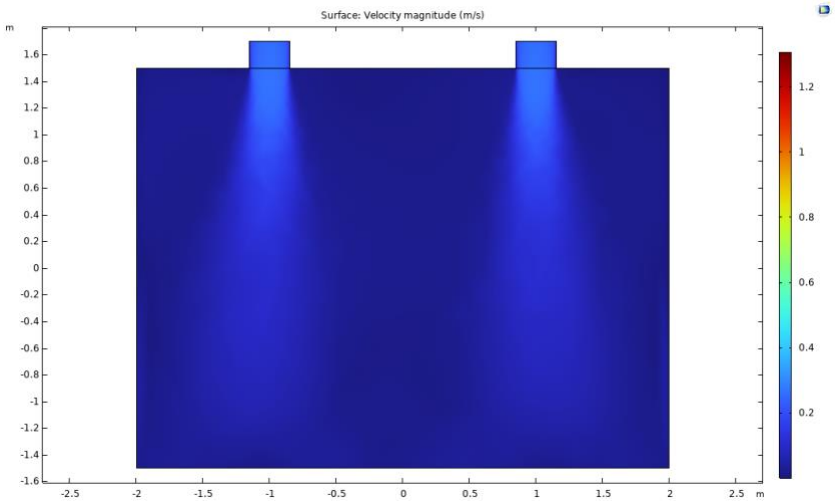

Figure 38. 2D Plot Surface xz plane, 2 ACH

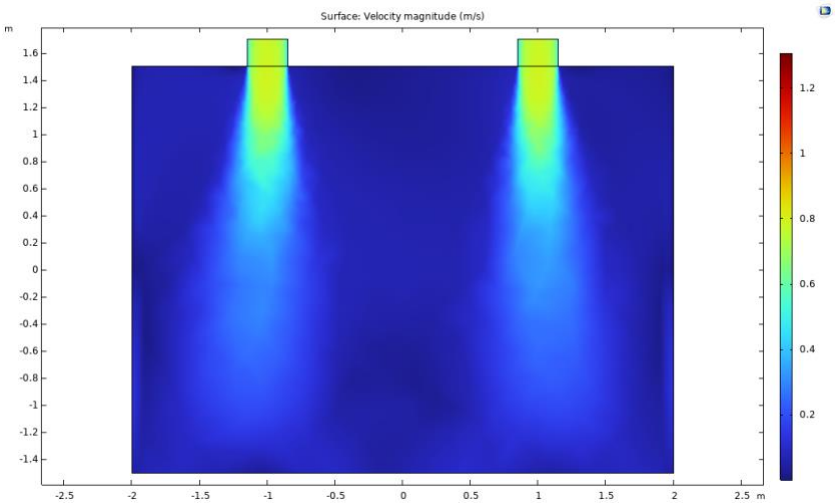

Figure 39. 2D Plot Surface xz plane, 6 ACH

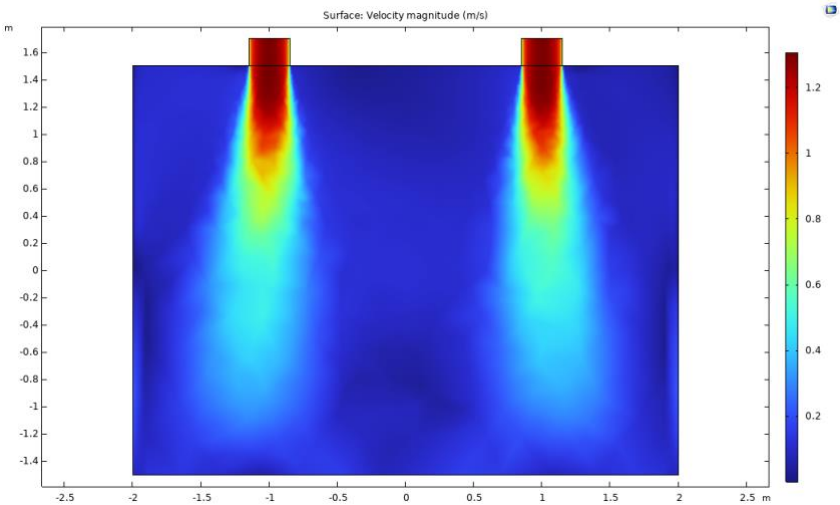

Figure 40. 2D Plot Surface xz plane, 10 ACH.

Figure 38-40. Comparison of velocity surface plots at different air change rates (2 ACH, 6 ACH and 10 ACH). Increasing ventilation rates enhance jet penetration, turbulence intensity and mixing efficiency, while reducing stagnant regions within the confined environment

The increased inlet velocity reinforces jet dominance, producing stronger shear layers and higher local turbulence intensity. The Reynolds number increases proportionally with ACH, confirming the linear scaling Re ∝ ACH, yet the resulting flow organisation does not evolve in a purely proportional way. The jets may extend more directly toward the outlet vents, establishing preferential pathways that partially bypass lateral mixing. Evidence of this directional dominance can be inferred from the streamline topology shown in figures,

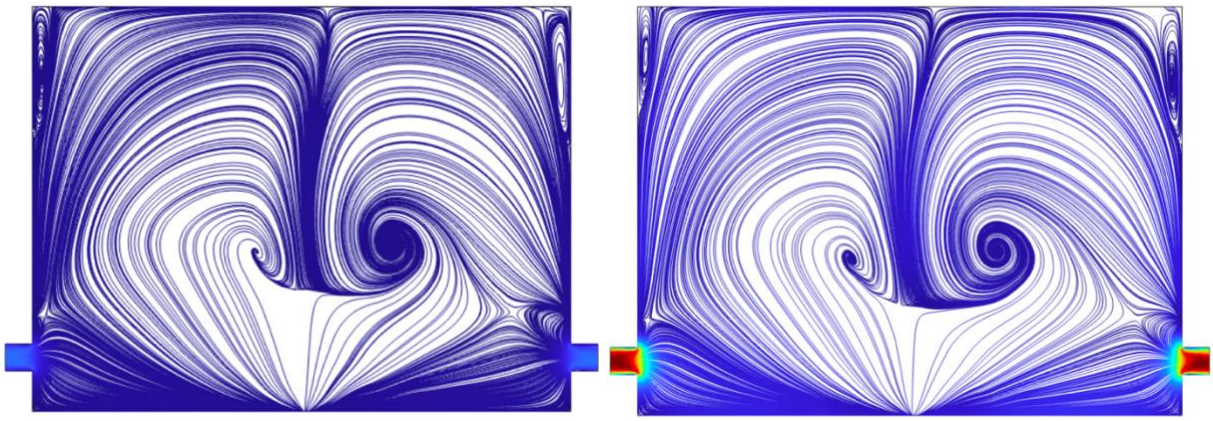

Figure 41. 10 ACH.

Figure 42. 2 ACH

Figure 41 and 42. Comparison of streamline topology for low and high ventilation rates. 2 ACH configuration characterised by weaker jet penetration and larger recirculation regions; 10 ACH configuration showing stronger directional jet structures, enhanced turbulence intensity and preferential flow pathways toward the outlet vents.

where the high-momentum core maintains coherence over longer distances. In such conditions, global residence time decreases significantly, in agreement with the exponential decay model $C(t) = C0\, e^{-ACH\, t}$ yet spatial heterogeneity may increase locally due to short-circuiting effects.

This apparent contradiction highlights a key aspect of ventilation-driven sanitisation: although the scaling between ACH and Reynolds number is linear, homogenisation efficiency does not follow the same proportionality. Increasing ventilation rate reduces theoretical clearance time and accelerates bulk air replacement, but it may simultaneously reinforce directional flow structures that limit cross-stream mixing.

The visual evidence provided by the geometric projections in figures 12 and 13 further supports the interpretation that vent positioning and obstacle arrangement influence the degree to which increased ACH translates into improved uniformity. These findings carry important practical implications. Simply increasing the ventilation rate does not automatically guarantee improved spatial uniformity of hydrogen peroxide vapour. Optimal sanitisation design therefore requires a balanced evaluation of jet penetration, turbulence intensity, obstacle interaction, and recirculation behaviour, rather than reliance on ACH as a single performance indicator.

4.4 Hydrogen Peroxide Vapour Distribution

The evolution of the hydrogen peroxide concentration field within the enclosure is governed by the transient convection–diffusion equation (eq. 31) which describes the combined effects of advection by the velocity field and molecular diffusion. In the present ventilation configurations, the scalar transport regime is characterised by a high Peclet number, defined as

$$Pe = u\frac{L}{D} \tag{43}$$

Given that Pe assumes values on the order of 10^5 under typical operating conditions, transport is strongly convection-dominated. This implies that the structure of the concentration field is primarily determined by the airflow topology, and diffusion plays only a secondary role at the scale of the room.

During the injection phase, high concentration regions initially develop in the vicinity of the inlet vents, where the prescribed scalar value enters the domain together with the turbulent jets. The vapour rapidly propagates along the jet trajectories, following the high-momentum cores that were previously discussed in connection with the

streamline representations. This behaviour can be interpreted in light of the velocity fields shown in figures 12 and 13, which clarifies the relative positioning of vents and obstacles, and in figure 35, where the dominant jet paths are clearly identifiable. As the jets entrain surrounding air and expand laterally, concentration spreads progressively into the bulk of the enclosure.

However, penetration into recirculation zones occurs with noticeable delay. The recirculating structures that form behind obstacles, particularly those illustrated in figure 37, create regions in which convective transport is weaker and scalar renewal is slower. In these shadowed areas, the concentration increase during injection is governed largely by turbulent mixing at shear layer interfaces rather than by direct jet impingement. As a result, significant spatial heterogeneity may persist during the early transient stage.

During the removal phase, once vapour injection ceases and ventilation continues, the theoretical well-mixed model predicts an exponential decay of concentration according to (eq. 41).

This expression, derived from a global mass balance under the assumption of instantaneous mixing, provides a convenient macroscopic reference. The CFD results indicate that, after sufficient time has elapsed for large-scale mixing to develop, the spatially averaged concentration within the enclosure follows this exponential decay reasonably well. This agreement confirms that the model correctly captures the overall mass exchange dynamics imposed by the ventilation rate.

Nevertheless, examination of the local concentration fields reveals substantial deviations from the perfectly mixed assumption, particularly during the initial stages of removal. While the global average may decrease smoothly in accordance with the exponential law, certain regions—especially those associated with persistent recirculation or weak flow—exhibit slower decay rates. The geometric projections presented in figures 12 and 13 help contextualise these local variations by showing how obstacle positioning influences flow confinement and scalar retention (Awbi, 2003).

These observations underscore the limitations of simple exponential decay models when used to predict local surface exposure. Although such models are adequate for estimating bulk clearance time, they cannot account for spatially resolved concentration gradients that determine the effective dose received by individual surfaces. The CFD framework therefore provides essential additional insight by revealing how transient convection patterns and geometric constraints shape the real distribution of hydrogen peroxide vapour within confined environments.

4.5 Comparison with Theoretical Flow Predictions

Validation of the numerical model was carried out through comparison with theoretical volumetric flow rates derived from the imposed inlet velocity distribution. The theoretical flow rate can be expressed as

$$P_{theoretical} = v \cdot A \tag{45}$$

where v represents the characteristic inlet velocity and A the total inlet surface area. This analytical estimate provides a direct reference against which the numerically evaluated flow rate at the outlet boundaries can be assessed. The relative deviation between theoretical and computed values was quantified as

$$\frac{|P_{theoretical} - P_{evaluated}|}{|P_{theoretical}|} \tag{46}$$

The results indicate that, in simulations employing the structured mesh configuration described in Chapter 3, this deviation remains minimal across refinement levels. Such

agreement confirms that mass conservation is correctly enforced within the computational domain and that the prescribed boundary conditions are implemented consistently. The importance of this verification step becomes particularly evident when considering the sensitivity of streamline coherence to discretisation quality, as previously illustrated in figures 35 and 36. A physically coherent flow field, free from artificial streamline termination, is a prerequisite for accurate global mass balance.

Further confidence in the numerical framework is obtained through comparison between the theoretical exponential decay model and the spatially averaged concentration obtained from the simulations. The decay law (eq. 45) derived under the assumption of perfect mixing, serves as a macroscopic benchmark. As discussed in connection with the geometric configuration shown in figures 12 and 13, the actual enclosure includes internal obstacles that generate local heterogeneity. Despite this geometric complexity, the averaged concentration predicted by the CFD model follows the theoretical exponential trend with good agreement once sufficient mixing has developed. This convergence between analytical prediction and numerical averaging supports the reliability of the solver and reinforces the consistency of the implemented transport equations.

Together, the close correspondence between theoretical and computed volumetric flow rates and the agreement between analytical decay and simulated average concentration demonstrate that the numerical model preserves both mass conservation and global dynamic behaviour, thereby providing a solid foundation for the detailed spatial analyses presented in the subsequent sections.

4.6 Sensitivity to Mesh and Numerical Parameters

The influence of mesh quality, extensively discussed in Chapter 3, becomes even more evident when analysing the scalar concentration field rather than the velocity field alone. In a convection-dominated regime, where the Péclet number is high and

transport is primarily driven by advection, any inaccuracy in the spatial discretisation directly affects the sharpness and physical credibility of concentration gradients. When mesh refinement is insufficient, shear layers that should appear well-defined tend instead to become artificially smoothed. This smoothing effect is not a physical phenomenon, but a manifestation of numerical diffusion introduced by inadequate element resolution. Consequently, concentration gradients may be underestimated, particularly in regions where high-momentum jets interact with slower ambient air or impinge upon obstacles.

Such behaviour can be interpreted in light of the streamline comparisons presented in figure 35 and 36. The reduced coherence observed in the unstructured mesh configuration does not merely affect the visual representation of flow trajectories; it propagates into the scalar field, diminishing the model's ability to capture sharp transitions between high- and low-concentration regions. Similarly, the geometric projections shown in figures 12 – 13 clarify how obstacle positioning can create confined regions in which accurate gradient resolution is essential for predicting local exposure.

The adoption of a structured mesh significantly reduces artificial numerical diffusion and preserves the fidelity of both velocity and concentration fields. By aligning elements with dominant flow directions and ensuring controlled growth ratios near boundaries, the structured discretisation maintains sharper shear interfaces and more realistic scalar transport patterns. This improvement is particularly relevant in regions adjacent to inlet jets and within recirculation zones, where concentration gradients are strongest.

In addition to spatial discretisation analysis, temporal convergence was assessed through time step sensitivity tests. The transient simulations employed an implicit backward differentiation formula (BDF) scheme, selected for its stability properties in stiff, advection-dominated problems. Progressive reduction of the time step revealed that, beyond a certain threshold, further refinement produced negligible variation in the temporal evolution of concentration. This behaviour confirms

temporal convergence and indicates that the numerical solution is not influenced by artificial oscillations or time discretisation errors.
Taken together, the spatial and temporal convergence analyses reinforce the robustness of the computational framework. The consistency observed across mesh refinement levels and time step variations supports the reliability of the predicted hydrogen peroxide vapour distribution and strengthens the physical interpretation of sanitisation dynamics within the mechanically ventilated enclosure.

4.7 Effect of substrate properties on hydrogen peroxide deposition

A further aspect of interest that emerged during the analysis of the results concerns the influence of the surface properties of materials on the distribution and deposition of vaporized hydrogen peroxide. Under the same operating conditions, different substrates exhibit significantly different behaviors with respect to the absorption and retention of the sanitizing agent.
In particular, porous materials tend to retain a greater quantity of hydrogen peroxide compared to non-porous materials or surfaces characterized by low roughness. This phenomenon is mainly related to the presence of microcavities, asperities, and internal porosity, which increase the effective surface area available for interaction with the airflow containing H_2O_2. Consequently, during the sanitization process, part of the hydrogen peroxide is adsorbed or condensed within the structure of the material, leading to locally higher surface concentrations within the same time interval.
Conversely, smooth plastic surfaces or low-porosity materials exhibit a lower retention capacity for hydrogen peroxide. In these cases, the transport of the chemical species is mainly governed by convective and diffusive surface phenomena, resulting in less intense and more uniform deposition. The reduced interaction with the

substrate also leads to a faster redistribution of the vapor within the surrounding environment.

From a fluid dynamic point of view, this behavior can be interpreted considering that turbulent flow transports hydrogen peroxide toward surfaces through mechanisms of molecular diffusion and convective transport; subsequently, the amount of species effectively deposited depends on the physicochemical characteristics of the material. Textile materials, wooden surfaces, or porous coatings may therefore act as temporary accumulation sites for the sanitizing agent, whereas compact polymeric surfaces exhibit a more reflective behavior toward the transported species.

The simulations and qualitative observations therefore suggest that the materials present inside the environment represent a non-negligible parameter in the definition of sanitization protocols. In the presence of highly porous surfaces, it may be necessary to increase either the exposure time or the initial H_2O_2 concentration in order to ensure the achievement of homogeneous disinfection levels throughout the treated volume. Conversely, environments mainly characterized by smooth and non-absorbing surfaces generally allow a faster and more uniform distribution of vaporized hydrogen peroxide.

4.8 Engineering Interpretation and Practical Implications

The numerical results offer direct and practically relevant engineering insight into the behaviour of hydrogen peroxide vapour in mechanically ventilated confined environments. One of the most evident conclusions concerns the influence of vent placement on recirculation topology. The geometric configuration illustrated in figures 12 and 13 demonstrates how the relative positioning of supply and outlet vents, together with internal obstacles, shapes the global flow pathways. The streamline visualisations presented in figure 37 further confirm that even slight geometric asymmetries may generate persistent recirculation zones behind obstacles. These regions, which emerge as a direct consequence of jet–wall and jet–obstacle

interaction, are not merely secondary features but decisive elements in determining local vapour transport and exposure time.

The analysis of varying ACH values reveals that moderate ventilation rates often produce the most balanced mixing conditions. At intermediate Reynolds numbers, jet penetration is sufficient to disrupt large stagnant zones while avoiding excessive directional dominance. This behaviour is consistent with the flow structures observed in figure 35, where structured mesh simulations show coherent yet well-dispersed streamline patterns. In contrast, when ACH becomes excessively high, the strengthened jet core may create preferential pathways between inlet and outlet vents, thereby accelerating bulk air replacement but potentially reducing lateral dispersion. The result is a decrease in global residence time accompanied by the persistence of local heterogeneity, as discussed in relation to the exponential decay model $C(t) = C0\, e^{-ACH\, t}$.

These observations underscore the value of CFD simulation as an indispensable tool for identifying stagnation zones and regions of delayed exposure that would remain undetected under a perfectly mixed assumption. While global mass balance models can estimate average clearance times, only spatially resolved simulations can reveal the detailed interaction between jet dynamics, obstacle-induced recirculation, and scalar transport.

The implications of these findings directly connect to the broader discussion developed in Chapter 1, where the importance of controlled hydrogen peroxide distribution was emphasised not only for hospital environments but also for offices, commercial spaces, and other confined settings. Effective sanitisation depends not solely on achieving a target concentration level but on ensuring that vapour reaches all relevant surfaces with adequate intensity and duration. Spatial and temporal distribution patterns therefore become as critical as concentration magnitude itself.

The present analysis demonstrates that ventilation design, jet structure, and geometric

configuration must be considered together in order to achieve reliable and uniform sanitisation performance.

4.9 Limitations of the Model

Although the present numerical framework provides robust and physically consistent insight into airflow and hydrogen peroxide vapour transport, certain limitations must be recognised in order to define the scope of validity of the results. The current formulation focuses exclusively on fluid dynamic transport phenomena and treats hydrogen peroxide as a passive scalar governed by advection and diffusion. As a consequence, chemical decomposition kinetics are not explicitly incorporated into the model. In real environments, hydrogen peroxide may undergo catalytic breakdown on certain materials or under specific environmental conditions, potentially altering concentration evolution over longer timescales.

Similarly, the interaction between vapour and solid surfaces is simplified through the imposition of impermeable boundary conditions with zero normal diffusive flux. While this assumption allows a clear interpretation of convective transport mechanisms, it neglects possible adsorption, desorption, or reactive processes occurring at walls and furniture surfaces. The geometric representations shown in figures 12 and 13, highlight the complexity of surface configurations within the enclosure; incorporating detailed surface chemistry would therefore introduce additional modelling challenges and require material-specific parameters.

The present approach also assumes a single-phase vapour without accounting for potential condensation or multiphase effects that could arise under high local concentration or specific thermodynamic conditions. In practical sanitisation scenarios, especially in confined regions such as those illustrated by the recirculation zones in 25, multiphase interactions may influence local deposition and effectiveness.

Furthermore, boundary conditions are idealised in the sense that inlet velocity profiles and outlet pressure references are prescribed deterministically, without

modelling possible fluctuations or uncertainties associated with real ventilation systems.

These simplifications were intentionally adopted to isolate and analyse the dominant convective transport mechanisms within a controlled and numerically stable framework. However, they define the limits within which the present conclusions should be interpreted. Future research could extend the model by incorporating reactive transport equations, surface interaction kinetics, and multiphase phenomena, thereby enabling a more comprehensive representation of hydrogen peroxide behaviour. In parallel, experimental validation campaigns carried out in geometries representative of the simulated enclosure would provide valuable empirical data for calibrating and refining the computational framework, thereby strengthening the correspondence between numerical predictions and real-world sanitisation conditions. Such developments would further strengthen the integration between computational modelling and practical sanitisation engineering.

4.10 Computational Requirements and Technological Limitations

The numerical investigation presented in this work highlighted not only the physical complexity associated with hydrogen peroxide vapour transport in confined environments, but also the significant computational requirements associated with high-fidelity CFD simulations. As the numerical model becomes progressively more detailed and physically representative, the computational cost increases rapidly, introducing important technological and practical limitations.

In the early stages of the study, relatively simplified simulations were performed using conventional single-processor workstations equipped with standard memory configurations. These initial computational resources were sufficient for preliminary analyses involving simplified geometries, moderate mesh densities, and stationary

flow conditions. However, as the model complexity increased, the limitations of such hardware configurations became progressively more evident.

The introduction of finer meshes, internal obstacles, boundary layer refinement, transient simulations, and coupled multiphysics transport significantly increased the number of degrees of freedom involved in the numerical solution. In particular, the adoption of time-dependent simulations required repeated solution of large non-linear systems over multiple temporal steps, with a substantial increase in memory allocation and computational time. Similarly, the implementation of refined structured meshes and localised mesh refinement near walls and inlet regions generated a dramatic increase in the total number of elements, directly affecting solver stability and convergence behaviour.

Additional complexity was introduced through the investigation of different ventilation regimes, inlet velocities, and material-dependent surface configurations. Variations in airflow intensity and geometric complexity generated increasingly articulated flow structures characterised by stronger recirculation zones, higher turbulence levels, and sharper scalar concentration gradients. Under such conditions, maintaining numerical stability while preserving physical accuracy required progressively more demanding computational resources.

For these reasons, the computational workflow evolved toward the use of more advanced hardware platforms. The later stages of the research were performed using high-performance workstations equipped with dual-processor architectures, high-memory GPU configurations, and RAM capacities exceeding 128 GB. These upgrades allowed the management of larger meshes, improved convergence behaviour, and reduced computational times for transient multiphysics simulations.

Nevertheless, even with advanced workstation configurations, important computational limitations remained. Highly refined simulations involving very fine meshes, complex obstacle distributions, transient turbulent transport, and detailed scalar resolution may still require High Performance Computing (HPC) infrastructures in order to achieve acceptable solution times and stable convergence.

This aspect represents one of the main technological gaps currently affecting the large-scale diffusion of advanced CFD methodologies in environmental sanitisation studies.

From a broader perspective, the present work demonstrates that the development of increasingly realistic CFD models is strongly dependent on the availability of adequate computational resources. The relationship between physical fidelity and computational cost therefore becomes a critical factor in model design. While simplified simulations may provide rapid qualitative information, physically accurate predictions of vapour transport and removal in realistic environments often require computational capabilities that are not always accessible due to financial constraints, hardware availability, or institutional limitations.

Consequently, future developments in this field will likely depend not only on advances in numerical modelling techniques, but also on the increasing accessibility of high-performance computational infrastructures capable of supporting large-scale multiphysics simulations for environmental engineering applications.

Chapter 5

5.1 Conclusions

This doctoral research has investigated the decontamination of confined indoor environments by means of vaporised hydrogen peroxide (VHP) through a Computational Fluid Dynamics (CFD) approach. The study has demonstrated that the effectiveness of VHP-based decontamination cannot be interpreted solely in terms of target concentration levels but must be understood as a coupled transport phenomenon governed by airflow structure, turbulence, and room geometry.

The numerical simulations have shown that vapour distribution is strongly influenced by the topology of the velocity field. In particular, recirculation zones, stagnation regions, and flow separation induced by internal obstacles lead to significant spatial heterogeneity in concentration fields. Therefore, surface exposure conditions are not uniform, and certain areas may experience reduced decontamination effectiveness due to local shielding and flow shadowing effects.

The analysis of ventilation rate further highlighted a non-linear relationship between air changes per hour (ACH) and vapour distribution. While increased ventilation enhances turbulent mixing and accelerates global distribution, it may also promote preferential flow pathways between inlet and outlet regions, reducing local residence time. This trade-off suggests that increasing ventilation alone is not sufficient to guarantee optimal decontamination performance.

The study has also emphasised the importance of the aeration phase. Although volume-averaged concentration decay follows trends comparable to ideal well-mixed models, local concentration fields exhibit significant spatial variability. Regions characterised by weak ventilation may retain higher concentrations for longer periods, potentially delaying safe re-entry. This finding highlights a limitation of approaches based solely on average concentration measurements.

A further relevant aspect concerns the phase following decontamination, namely the removal of residual hydrogen peroxide and the subsequent restoration of safe conditions for the re-entry of operators into the confined environment. In this case as well, the nature of the substrate significantly influences system behaviour. Porous materials are expected to retain larger amounts of H_2O_2 due to adsorption and penetration phenomena occurring within the material structure, prolonging the persistence of residual concentrations within the environment. This phenomenon may result in longer aeration times before the hydrogen peroxide concentration falls below the safety thresholds established for human exposure.

Conversely, smooth and poorly absorbent surfaces promote a faster removal of residual hydrogen peroxide, since the amount retained by the material is lower and

the compound mainly remains in the gaseous phase, where it can be more easily removed through ventilation and air exchange. Consequently, environments characterised by a greater presence of plastic or metallic materials generally exhibit shorter operational recovery times compared to environments containing textile, wooden, or highly porous materials.

From an applicative perspective, these considerations are particularly important in the design of biodecontamination protocols, as they highlight the need to adapt aeration times and ventilation strategies not only according to the room volume and the initial H_2O_2 concentration, but also according to the properties of the materials present within the treated domain. The combined evaluation of deposition, adsorption, release, and removal of the sanitising agent therefore represents a fundamental aspect in ensuring both the microbiological effectiveness of the treatment and the safety of the environment after decontamination.

These results therefore demonstrate that decontamination effectiveness does not exclusively depend on the fluid dynamic conditions of the flow or on the geometry of the environment, but also on the properties of the materials present within the computational domain. The integration of models capable of accounting for surface adsorption, desorption phenomena, and vapour–substrate interactions therefore represents a particularly relevant future development for improving the realism of CFD simulations applied to indoor biodecontamination processes.

From a methodological perspective, the integration of CFD modelling with transport of diluted species has enabled a detailed and spatially resolved analysis of both distribution and removal phases. The adoption of a turbulence modelling framework based on the SST k–ω model has ensured a reliable representation of both near-wall behaviour and free-stream flow structures, which are critical for realistic indoor simulations.

Overall, the main contribution of this research lies in the development of a unified computational framework capable of capturing the multiphysics nature of VHP decontamination in confined environments. By explicitly linking airflow dynamics,

scalar transport, and spatial variability of exposure conditions, the study provides a more comprehensive understanding compared to simplified or purely experimental approaches.

5.2 Limitations of the Study

Despite the robustness of the proposed modelling approach, several limitations must be acknowledged.

First, hydrogen peroxide vapour has been treated as a passive scalar, neglecting potential chemical decomposition and surface reactions. While this assumption is justified for short time scales and low reactivity conditions, it may not fully capture all physical processes involved in real decontamination scenarios.

Second, the analysis has been conducted on a simplified geometric configuration representing a confined indoor environment. Although the inclusion of obstacles enhances realism, actual environments may present additional complexities, such as variable ventilation systems, thermal effects, and human presence.

Third, the study has focused on concentration fields as a proxy for decontamination effectiveness, without explicitly modelling microbial inactivation kinetics. As a result, the link between vapour exposure and biological efficacy remains indirect.

5.3 Future Developments

Future research should aim to extend the present framework in several directions.

A first development concerns the inclusion of reactive transport mechanisms, allowing simulation of hydrogen peroxide decomposition and interaction with surfaces. This would provide a more accurate representation of decontamination processes, particularly in environments with high humidity or catalytic materials.

A second improvement involves coupling CFD simulations with microbial inactivation models, enabling a direct assessment of decontamination effectiveness rather than relying solely on concentration fields.

From a geometrical perspective, further studies should investigate more complex and realistic indoor environments, including multi-room configurations, different ventilation layouts, and transient occupancy conditions.
Finally, experimental validation of the numerical results represents a crucial step for strengthening the predictive capability of the model. The integration of CFD simulations with experimental measurements would allow calibration and verification of both airflow and concentration fields.

Bibliography

[1] Klepeis, N. E., Nelson, W. C., Ott, W. R., Robinson, J. P., Tsang, A. M., Switzer, P., Behar, J. V., Hern, S. C., Engelmann, W. H. (2001). *The National Human Activity Pattern Survey (NHAPS): a resource for assessing exposure to environmental pollutants*. Journal of Exposure Analysis and Environmental Epidemiology, 11(3), 231–252.

[2] World Health Organization (WHO) (2011*). Report on the Burden of Endemic Health Care-Associated Infection Worldwide*. WHO Press, Geneva.

[3] European Centre for Disease Prevention and Control (ECDC) (2019). *Healthcare-associated infections: prevalence and prevention*. ECDC Report.

[4] Morawska, L., Cao, J. (2020). *Airborne transmission of SARS-CoV-2: The world should face the reality*. Environment International, 139, 105730.

[5] Kramer, A., Schwebke, I., Kampf, G. (2006). *How long do nosocomial pathogens persist on inanimate surfaces?* BMC Infectious Diseases, 6, 130.

[6] Otter, J. A., Yezli, S., French, G. L. (2013). *The role played by contaminated surfaces in the transmission of nosocomial pathogens.* Infection Control & Hospital Epidemiology, 34(5), 449–456.

[7] Hall-Stoodley, L., Costerton, J. W., Stoodley, P. (2004*). Bacterial biofilms: from the natural environment to infectious diseases.* Nature Reviews Microbiology, 2(2), 95–108.

[8] Carling, P. C., Parry, M. F., Von Beheren, S. M. (2008). *Identifying opportunities to enhance environmental cleaning in hospitals.* Infection Control & Hospital Epidemiology, 29(1), 1–7.

[9] World Health Organization (WHO) (2023). *Antimicrobial resistance global report*. WHO.

[10] Linley, E., Denyer, S. P., McDonnell, G., Simons, C., Maillard, J. Y. (2012). *Use of hydrogen peroxide as a biocide: new consideration of its mechanisms of biocidal action.* Journal of Antimicrobial Chemotherapy, 67(7), 1589–1596.

[11] McDonnell, G., Russell, A. D. (1999*). Antiseptics and disinfectants: activity, action, and resistance*. Clinical Microbiology Reviews, 12(1), 147–179.

[12] Otter, J. A., Yezli, S., Perl, T. M., Barbut, F., French, G. L. (2007). *The role of 'no-touch' automated room disinfection systems in infection prevention and control*. Journal of Hospital Infection, 65, 1–13.

[13] Occupational Safety and Health Administration (OSHA) (2023). *Hydrogen Peroxide: Occupational Exposure Limits.* OSHA Guidelines.

[14] Hall, L., Otter, J. A., Chewins, J., Wengenack, N. L. (2007). *Use of hydrogen peroxide vapor for deactivation of Mycobacterium tuberculosis in a biological safety cabinet*. Journal of Clinical Microbiology, 45(3), 810–815.

[15] Boyce, J. M., Havill, N. L., Otter, J. A., McDonald, L. C., Adams, N. M., Thompson, A. (2008). *Impact of hydrogen peroxide vapor room decontamination on Clostridium difficile infection rates.* Infection Control & Hospital Epidemiology, 29(8), 723–729.

[16] Awbi, H. B. (2003). *Ventilation of Buildings*. 2nd Edition, Spon Press.

[17] Chen, Q. (2009). *Ventilation performance prediction for buildings: A method overview and recent applications*. Building and Environment, 44(4), 848–858.

[18] Nielsen, P. V. (2015). *Fifty years of CFD for room air distribution.* Building and Environment, 91, 78–90.

[19] Agency for Toxic Substances and Disease Registry (ATSDR) (2002). *Toxicological Profile for Hydrogen Peroxide.* U.S. Department of Health and Human Services.

[20] Hamner, L., Dubbel, P., Capron, I., et al. (2020). *High SARS-CoV-2 attack rate following exposure at a choir practice.* MMWR, 69(19), 606–610.

[21] Versteeg, H. K., Malalasekera, W. (2007). *An Introduction to Computational Fluid Dynamics: The Finite Volume Method*. 2nd Edition, Pearson.

[22] Hinze, J. O. (1975). *Turbulence.* 2nd Edition, McGraw-Hill.

[23] Pope, S. B. (2000). *Turbulent Flows.* Cambridge University Press.

[24] Wilcox, D. C. (2006). *Turbulence Modeling for CFD.* DCW Industries.

[25] Wilcox, D. C. (1988). *Reassessment of the scale-determining equation for advanced turbulence models.* AIAA Journal, 26(11), 1299–1310.

[26] Launder, B. E., Spalding, D. B. (1974). *The numerical computation of turbulent flows*. Computer Methods in Applied Mechanics and Engineering, 3(2), 269–289.

[27] Menter, F. R. (1994). *Two-equation eddy-viscosity turbulence models for engineering applications.* AIAA Journal, 32(8), 1598–1605.

[28] Zienkiewicz, O. C., Taylor, R. L. (2000). *The Finite Element Method.* Butterworth-Heinemann.

[29] Ferziger, J. H., Perić, M. (2002). *Computational Methods for Fluid Dynamics.* Springer.

[30] Bird, R. B., Stewart, W. E., Lightfoot, E. N. (2002). *Transport Phenomena*. 2nd Edition, Wiley.

[31] Noakes, C. J., Sleigh, P. A., Beggs, C. B., Kerr, K. G. (2006). *Modelling the transmission of airborne infections in enclosed spaces*. Epidemiology and Infection, 134(5), 1082–1091.

[32] White, F. M. (2006). *Viscous Fluid Flow.* 3rd Edition, McGraw-Hill.

[33] Fox, R. W., McDonald, A. T., Pritchard, P. J. (2011). *Introduction to Fluid Mechanics.* 8th Edition, Wiley.